

# Combined Quantum Mechanical and Molecular Dynamics study of paramagnetic complexes

Towards an understanding of electronic spin relaxation

Shehryar Khan

Academic dissertation for the Degree of Doctor of Philosophy in Chemical Physics at Stockholm University to be publicly defended on Tuesday 12 June 2018 at 13.00 in FB53, AlbaNova Universitetscentrum, Roslagstullsbacken 21.

## Abstract

The prime objectives of contrast agents in Magnetic Resonance Imaging (MRI) is to accelerate the relaxation rate of the solvent water protons in the surrounding tissue. Paramagnetic relaxation originates from dipole-dipole interactions between the nuclear spins and the fluctuating magnetic field induced by unpaired electrons. Currently Gadolinium(III) chelates are the most widely used contrast agents in MRI, and therefore it is incumbent to extend the fundamental theoretical understanding of parameters that drive the relaxation mechanism in these complexes. In compounds such as Gadolinium(III) complexes with total electron spins higher than 1 (in this case  $S=7/2$ ) the Zero-Field Splitting (ZFS) plays a significant role in influencing the electron spin dynamics and nuclear spin dynamics. For this purpose, the current research delves into an understanding of the relaxation process, focusing on ZFS in various complexes of interest, using multi-scale modelling by combining quantum, semi-quantum and newtonian methods.

We compare and contrast Density Function Theory (DFT) with multi-configurational quantum chemical calculation and find that DFT is highly functional dependent and unreliable in accurately reproducing experimental data for the static ZFS. It was found that long-range corrected functionals (in particular LC-BLYP) perform significantly better as compared to other functionals in predicting the magnitude of the static ZFS. We study hydrated Gd(III) and Eu(II) systems to compare and contrast these isoelectronic complexes (both contain 7 unpaired electrons in their valence shell) and through ab-initio molecular dynamics (AIMD) sampling followed by multi-reference quantum chemical calculations, it was established that inclusion of the first shell has a dominant influence (over 90%) on the ZFS. We also studied the complex [Gd(III)(HPDO3A)(H<sub>2</sub>O)], which is of clinical relevance as a contrast agent for MRI, through post-Hartree-Fock and DFT calculations by utilizing configurations derived from AIMD trajectories. From the fluctuations in the ZFS tensor, we extract a correlation time of the transient ZFS which is on the sub-picosecond time scale, showing a faster decay than experimental data.

**Keywords:** *molecular dynamics, quantum chemistry, zero-field splitting.*

Stockholm 2018

<http://urn.kb.se/resolve?urn=urn:nbn:se:su:diva-155519>

ISBN 978-91-7797-320-1  
ISBN 978-91-7797-321-8



Stockholm  
University

Department of Physics

Stockholm University, 106 91 Stockholm



COMBINED QUANTUM MECHANICAL AND MOLECULAR  
DYNAMICS STUDY OF PARAMAGNETIC COMPLEXES

Shehryar Khan



# Combined Quantum Mechanical and Molecular Dynamics Study of Paramagnetic Complexes

Towards an understanding of electron spin relaxation

Shehryar Khan

©Shehryar Khan, Stockholm University 2018

ISBN print 978-91-7797-320-1  
ISBN PDF 978-91-7797-321-8

The front cover image was created with POV-Ray: <http://povray.org>  
Printed in Sweden by Universitetservice US-AB, Stockholm 2018  
Distributor: Department of Physics, Stockholm University

# List of Papers

The following papers, referred to in the text by their Roman numerals, are included in this thesis.

PAPER I: **Systematic theoretical investigation of the zero-field splitting in Gd(III) complexes: Wave function and density functional approaches**

S. Khan, A. Kubica-Misztal, D. Kruk, J. Kowalewski, M. Odelius

*J. Chem. Phys.*, **142**, 034304 (2015).

DOI: <http://dx.doi.org/10.1063/1.4905559>

PAPER II: **An ab initio CASSCF study of Zero Field Splitting Fluctuations in the Octet Ground State of Aqueous [Gd(III)(HPDO3A)(H<sub>2</sub>O)]**

S.Khan, R. Pollet, R. Vuilleumier, J. Kowalewski, M. Odelius

*J. Chem. Phys.*, **147**, 244306 (2017).

DOI: <https://doi.org/10.1063/1.5010347>

*Selected as Editor's pick*

PAPER III: **Zero-field splitting in the isoelectronic aqueous Gd(III) and Eu(II) complexes from a first principles analysis.**

S.Khan, V. Peters, J. Kowalewski, M. Odelius

*Chem. Phys.*, **503**, 56-64 (2018).

DOI: <https://doi.org/10.1016/j.chemphys.2018.02.002>

PAPER IV: **A complete normal mode analysis of the Zero-Field Splitting in paramagnetic hexa-aqua Mn(II) and Ni(II) complexes.**

S.Khan, J. Kowalewski, M. Odelius

*In manuscript*

---

Reprints were made with permission from the publishers.

# Author's contribution

PAPER I: I shared responsibility for writing and organizing the manuscript and had the main responsibility for the ZFS computations.

PAPER II: I shared responsibility for writing and organizing the manuscript and had the main responsibility for the ZFS computations.

PAPER III: I shared responsibility for writing and organizing the manuscript and had the main responsibility for the ZFS computations. The extended sampling of the Gd(III) complex was performed by Vivian Peters.

PAPER IV: I shared responsibility for writing and organizing the manuscript and had the main responsibility for the ZFS computations.

PAPER I and III were included in my licentiate thesis and parts of the background, in particular the theoretical background chapters (Chapters 2 and 3) are based upon the licentiate degree. Parts of Chapter 4 appeared in the licentiate as well, but have been rearranged into different sections.



# Contents

<b>List of Papers</b>	<b>i</b>
<b>Author's contribution</b>	<b>iii</b>
<b>List of Abbreviations</b>	<b>vii</b>
<b>1 Introduction</b>	<b>9</b>
<b>2 Molecular Quantum Mechanics</b>	<b>15</b>
2.1 Introduction . . . . .	15
2.2 Wavefunction and Density Functional methods . . . . .	17
2.2.1 Hartree-Fock and CASSCF . . . . .	17
2.2.2 Density Functional Theory . . . . .	20
2.3 Relativistic Quantum Mechanics . . . . .	23
2.3.1 The Dirac Equation . . . . .	24
2.3.2 ZORA approximation . . . . .	24
2.3.3 DKH approximation . . . . .	25
2.4 ZFS and the Spin Hamiltonian formalism in Gd(III) complexes	26
<b>3 Nuclear Magnetic Resonance and Spin Relaxation</b>	<b>29</b>
3.1 Contrast agents for MRI scans . . . . .	29
3.2 Basic physics behind NMR . . . . .	30
3.3 Nuclear Spin Relaxation . . . . .	31
3.3.1 Dipole-Dipole Interactions . . . . .	32
3.3.2 Chemical Shift Anisotropy . . . . .	33
3.4 Paramagnetic effects in NMR . . . . .	33
3.4.1 Paramagnetic Relaxation Enhancement . . . . .	33
3.4.2 Pseudocontact Shift . . . . .	34
3.4.3 Residual Dipolar Couplings . . . . .	34
3.5 Electron spin relaxation parameters from First-Principle Molecular Dynamics . . . . .	35

<b>4</b>	<b>Summary of Results</b>	<b>37</b>
4.1	Symmetrical systems: $O_h$ and $T_h$ symmetry . . . . .	37
4.1.1	ZFS in symmetrical Gd(III) systems . . . . .	37
4.1.2	ZFS associated with vibrational motion of aqueous Ni(II) and Mn(II) . . . . .	40
4.2	ZFS parameters from Density Functional Theory . . . . .	42
4.3	Paramagnetic ions in water: Aqueous Gd(III) and Eu(II) . . .	44
4.3.1	Comparing the Zero-Field splitting for the isoelectronic aqueous Gd(III) and Eu(II) . . . . .	44
4.3.2	AIMD trajectory: Comparison of inner and outer shell in aqueous Gd(III) . . . . .	47
4.4	Paramagnetic Complexes of Clinical Relevance . . . . .	47
4.4.1	Static ZFS in Gd(III)DOTA(H <sub>2</sub> O) <sup>-</sup> and Gd(III)DTPA(H <sub>2</sub> O) <sup>2-</sup> . . . . .	47
4.4.2	Static and Transient ZFS in Gd(III)(HPDO3A)(H <sub>2</sub> O): combining classical and quantum methods . . . . .	51
<b>5</b>	<b>Conclusions and Outlook</b>	<b>55</b>
	<b>Acknowledgements</b>	<b>lix</b>
	<b>Populärvetenskaplig sammanfattning</b>	<b>lxi</b>
	<b>References</b>	<b>lxiii</b>

# List of Abbreviations

<b>AIMD</b>	Ab-initio Molecular Dynamics
<b>BO</b>	Born-Oppenheimer
<b>CASSCF</b>	Complete Active Space Self-Consistent Field
<b>CI</b>	Configuration Interaction
<b>CP</b>	Coupled-Perturbed
<b>CSA</b>	Chemical Shift Anisotropy
<b>DFT</b>	Density Functional Theory
<b>DKH</b>	Douglas Kroll Hess
<b>FPMD</b>	First-principles Molecular Dynamics
<b>KS-DFT</b>	Kohn-Sham Density Functional Theory
<b>MCSCF</b>	Multi-Configurational Self-Consistent Field
<b>MD</b>	Molecular Dynamics
<b>MRI</b>	Magnetic Resonance Imaging
<b>NEVPT</b>	n-electron valence state perturbation theory
<b>NMR</b>	Nuclear Magnetic Resonance
<b>PK</b>	Pederson-Khanna
<b>pNMR</b>	paramagnetic Nuclear Magnetic Resonance
<b>PRE</b>	Paramagnetic Relaxation Enhancement
<b>QC</b>	Quantum Chemistry
<b>RDF</b>	Radial Distribution Function

<b>SI</b>	State Interaction
<b>ZFS</b>	Zero-Field Splitting
<b>ZORA</b>	Zeroth-Order Regular Approximation

# 1. Introduction

Until the 1960's physics and chemistry relied purely on theory and experiment. These are still often looked upon (by the general population) as the two main facets of science. One has a theory about a particular phenomena, and then it is upto either the theoretician or the experimentalist to come up with different consequences of that theory so that it is quantifiable and can be checked by experiments. On the other hand, in some cases, experiments at the cutting edge of what is technologically possible may drive new theories to develop.

However, with the advent of computational science, since the 1960's simulations have begun to move in as the third important facet of science. Computational methods become a tool for theorists and experimentalists and it is becoming increasingly essential for both to either have computational knowledge or at the very least collaborate with computational scientists. When we talk about the theoretical chemist or the theoretical condensed matter physicist for example, we instinctively assume that the scientist in these fields must be well versed in both theory as well as the computational aspects involved. A second feature of computation is that it is in essence a kind of experimental device for the theoretician (and vice versa for the experimentalist) but not restricted by the limitations that actual equipment may pose. This means it is possible to play around with your codes and increase or decrease various variables to extremes just to see what would happen, or create molecules that are theoretically possible but not experimentally yet viable. In this thesis, for example, we consider some idealized Gadolinium(III) complexes that are not experimentally viable but help us to gain various insights into the nature of some properties of more complex systems, which are relevant as contrast agents for Magnetic Resonance Imaging (MRI).

Aneesur Rahman, the Indian scientist from Hyderabad, in the 60's pioneered the implementation of the first Molecular Dynamics (MD) simulations on a system of 864 Argon atoms meant to depict it in the liquid state [1], and is often referred to as the father of MD. That paper was seminal in setting the stage for future MD simulations and formed the basis for many of the algorithms still used today. At around the same time Walter Kohn began to instigate the development of algorithms for computing the electronic

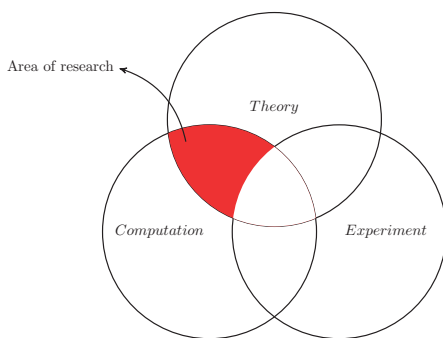


**Figure 1.1:** The three facets of science and the area of research I am mostly interested in. The area caught my interest due to its broad range of applications. Applied to paramagnetic NMR one is able to tackle theory from classical, semi-classical and quantum methods and so get a variety of experience to benefit from.

structure using information from just one parameter: the electron density, rather than the many-body wavefunction [2]. For his work he was awarded the Nobel Prize in Chemistry in 1998, an honour that he was slightly surprised by, since he had a strong background in physics and mathematical physics, though his work began to be used extensively by chemists. Currently the state of computational science has developed much farther than it had before, as computational power has been ascending exponentially and therefore allows the limits of increasingly complex systems to be computed. On top of computational efficiency, better theories, approximations and algorithms have been formed to derive properties that would simply not have been possible to calculate 50 years ago. However, we are nowhere near reaching the end of what is computationally possible, and the future, especially with the advent of quantum computing, looks very promising.

In this thesis, I discuss theoretical and computational approaches to calculate one property, the Zero-Field Splitting (ZFS) that is directly linked to the electronic structure of a paramagnetic complex. ZFS is a second-order effect of the spin-orbit coupling of a complex molecule. It influences the electron spin relaxation which in turn affects the nuclear spin relaxation through a phenomena known as paramagnetic relaxation enhancement (PRE). Since the 1980's it has been found that for a particular property of a molecule (the electronic spin  $S$ ), if it is greater than a certain value, then the phenomena of ZFS starts to play a dominating role. In larger atoms, electrons begin to approach the speed of light which suggests that Einstein's theory of relativity must be taken into account. The ZFS is a relativistic effect and simply means

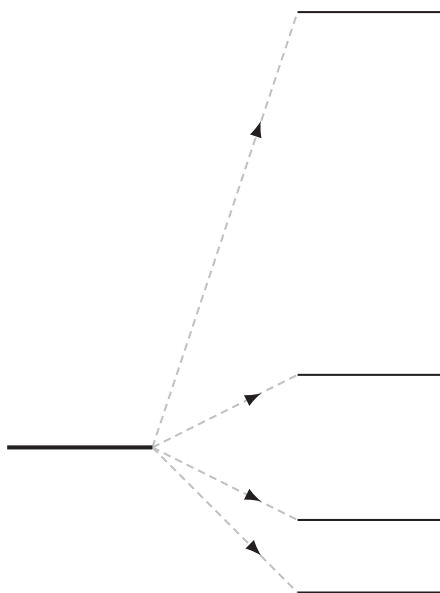


**Figure 1.2:** The splitting of degenerate electronic energy levels due to relativistic effects, at 0 magnetic field is what is known as the Zero-Field Splitting (ZFS). This is as opposed to the Zeeman effect where energy levels are split due to the presence of an external magnetic field. The diagram shows a schematic picture of the ground state energy levels being split of a Gd(III) complex, where there are 8 degenerate electronic energy levels. The introduction of a magnetic field induces further splitting into 8 nondegenerate spin states.

that the lowest degenerate energy levels, rather than all be equal in magnitude are split into various energy levels (refer to Fig. 1.2). This splitting of the ground state energy levels, in many atomic centres is extremely small. For example in a Nickel(II) complex the splitting can be higher than  $20 \text{ cm}^{-1}$  but for Gadolinium(III) complexes a typical value may be  $0.4 \text{ cm}^{-1}$ . Even though the value is extremely small the ZFS in Gd(III) complexes was found to have a profound effect on the electronic spin relaxation. The static ZFS plays a key role in PRE for many systems whose study is still relatively nascent and so not quite well understood, being a theoretically challenging subject.

Any theoretical scientist will always have two or more theories at his disposal when dealing with a particular subject. Even though the theories may be philosophically extremely different, they somehow could arise at the correct result for the property one is observing. Take for instance the philosophies behind wave-function methods and density-functional methods. The fundamental truths behind each of these methods are extremely different

and a small change in a parameter in one may lead to a drastic change in results for the other. Yet, it is clearly important to work with both methods within the framework of quantum theory at the moment. This is due to the fact that wave-function methods provide more accurate data, yet density-functional methods are much more computationally economical to perform and so if the scale of error is small it may be more efficient to work with the latter method. In PAPERS I and III, we show that density functional methods fail to provide accurate results when computing the static ZFS of complex Gadolinium(III) systems and are unreliable. Instead, we must use wave-function methods (in particular the complete-active space self-consistent field (CASSCF) method is used) to accurately reproduce the correct experimental ZFS parameters. Similarly in electronic spin relaxation theory there are currently four or five different models that have different philosophies behind them (as well as their own deficiencies) and yet can lead to similar results.

My motivation behind this thesis is two-fold. Firstly, to try and understand some of the theories in use today and the direction they are heading towards, relative to the electronic spin relaxation. Secondly, to make a small contribution to the field, no matter how tangential. The thesis aims to derive paramagnetic NMR properties, including (and specifically) static and time-dependent ZFS, from first principles and has the following objectives: wave-function and density functional methods are used to first calculate the ZFS for an idealized system followed by an investigation of the same methodology for more complex systems. The results of each method are then validated by comparing with experimental data. In addition the impacts of changes in various exogenous parameters such as structural distortions, solvent effects and dynamical influences are also investigated.

As shown in Fig. 1.3, for idealized systems which are perfectly symmetrical there is no zero-field splitting (ZFS). As we distort the symmetry in particular ways the energy levels are split and this induces ZFS. This distortion is studied axially as in PAPER I and along the normal vibrational modes as is performed in PAPER IV. This is important because often theoreticians start with an idealized geometry but in a temporal system (which is what happens in real life and experiments of course) the molecule will undergo distortions and therefore there will be a 'transient' ZFS associated with it that has to be taken into account. We show this, by running a time-dependent simulation (using First Principles Molecular Dynamics (FPMD)) and calculating the average (or static) ZFS and transient ZFS parameters associated with various systems using the CASSCF method. These types of calculations have never been performed before with such a high level



**Figure 1.3:** An idealised system  $\text{Gd(III)F}_6^{3-}$ , which has  $O_h$  symmetry will have no ZFS associated with it. However, if we distort the top and bottom atoms then the ground state degenerate energy levels will be split and ZFS begins to emerge.

of accuracy for lanthanide systems (PAPER II).

When computing large systems what it is possible to consider quantum mechanically is extremely limited. For example in a system of a 100 molecules we only consider 8 molecules (the inner core shell) quantum mechanically and the rest are treated by Newtonian physics, with continuum models or are completely ignored. We showed that this gives almost identical results if you include upto 26 molecules in the system (the second shell of the system). In other words it is sufficient for calculation of the ZFS just to include the first shell, and the additional computational and theoretical effort of including both the first and second shell is much more demanding and the results almost identical. This is shown in Fig. 1.4 (PAPER III). We show that a particular method (density functional theory) is unreliable at predicting values for the ZFS and even though a lot of literature uses this method, it fails to accurately predict the static ZFS, and a different method (wave-function theory) should be used. Furthermore, there is little or no correlation between the two methods (PAPERS I and II).

The dissertation is organized in four further chapters. The second chapter presents some of the basic theories used in quantum chemistry and Chapter 3 deals with the theories behind Nuclear Magnetic Resonance (NMR) spectroscopy so that one can familiarize themselves with the terms and methodologies used. Chapter 4 describes the summary of results that have been obtained. I discuss FPMD and *ab-initio* Quantum Chemical

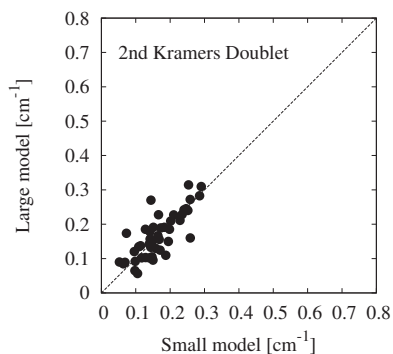


**Figure 1.4:** The figure depicts energies of the 2nd Kramers doublet using a small (x-axis) and large (y-axis) model. A comparison between inclusion of small and large model (which refers to the first and second shell respectively) of the lowest energy level shows an almost 1 to 1 correspondence in hydrated Gd(III) which is of prime importance when computing the ZFS. The graph is related to Paper III.

calculations performed on Gd(III) complexes (as well as Ni(II), Mn(II) and Eu(II) complexes) starting from simple structures to more complex ones. In particular the subject of ZFS is tackled from several different angles. The final chapter presents the conclusions.

# 2. Molecular Quantum Mechanics

## 2.1 Introduction

One of the founding principles on which a large part of modern science is based, is a consequence of the famous equation first written down in 1926, known as the time-dependent Schrödinger Equation:

$$\hat{\mathcal{H}}|\Psi(t)\rangle = i\hbar \frac{\partial}{\partial t} |\Psi(t)\rangle \quad (2.1)$$

This equation was born out of the mind of the Austrian scientist Erwin Schrödinger and for the first time laid down a description of how the wavefunction  $|\Psi(t)\rangle$  changes over time, through the Hamiltonian operator  $\hat{\mathcal{H}}$ , which represents the energy of a molecule or atom, and is a sum of kinetic and potential energy operators. Physical properties that remain constant over time can be described by the time-independent Schrödinger Equation:

$$\hat{\mathcal{H}}|\psi\rangle = E|\psi\rangle \quad (2.2)$$

which is an energy eigenvalue problem, where  $\psi$  are eigenstates of the Hamiltonian, and the total energy of the system in a particular state is given by the energy eigenvalue  $E$ . In a molecular system, the Hamiltonian includes kinetic and potential energy operators, the latter containing the electrostatic interaction between particles:

$$\hat{\mathcal{H}} = \hat{T}_N + \hat{\mathcal{H}}_e \quad (2.3)$$

$$\hat{\mathcal{H}}_e = \hat{T}_e + \hat{V}_{Ne} + \hat{V}_{ee} + \hat{V}_{NN} \quad (2.4)$$

$\hat{T}_N$  is the kinetic energy operator for the nuclei and  $\hat{T}_e$  is the kinetic energy operator for the electrons.  $\hat{V}_{Ne}$  represents the electrostatic attraction between electrons and nuclei,  $\hat{V}_{ee}$  represents the electrostatic repulsion between electrons, and  $\hat{V}_{NN}$  the electrostatic repulsion between nuclei. The solutions to Equation 2.2 give us a set of eigenfunctions which are associated with energy eigenvalues describing different quantum states of the system. With

this equation, we are capable of explaining a huge amount of atomic and molecular phenomena accurately and quantitatively, except those involving magnetism and relativity. However, even though it is a starting point for any electronic phenomenon, the complexity of the problem increases exponentially with each additional particle, and this places a severe limitation not only on computation, but in fact, the mathematics involved inherently in the problem becomes too complicated to solve analytically as soon as we go on to systems of atoms even with as little as two electrons.

Since the Schrödinger Equation was first written down in the 1920's, a whole range of techniques and approximations has been developed to provide reasonable computations for phenomena that occur in atomic and molecular systems. To circumvent some of the high dimensionality of the Schrödinger Equation, the Born-Oppenheimer approximation was proposed by Max Born and Robert J. Oppenheimer in 1927 [3], which is now often treated almost ubiquitously in wave function calculations. Since the nuclear mass is much greater than the electronic mass, the motion associated with the kinetic energy of nuclei is much slower than the electrons. When solving for the electronic wavefunction, the nuclei are essentially static and the inter-nuclear repulsion thus becomes a constant contribution to the Hamiltonian. Simplistically, in Equation 2.3 the term  $\hat{T}_N=0$ , so that only the electronic Hamiltonian is considered. The nuclear and electronic motions are thus separated and we can search for the solutions of the Schrödinger Equation separately:

$$\Psi_{total}(r;R) = \Psi_{nuclear}(R) \times \Psi_{electronic}(r;R) \quad (2.5)$$

where  $r$  represents electronic coordinates and  $R$  represents all nuclear coordinates. The electronic wavefunction of the Schrödinger Equation under the Born-Oppenheimer approximation is given by:

$$\hat{H}_{el}\Psi_{el}(r;R) = E_{el}\Psi_{el}(r;R) \quad (2.6)$$

The Born-Oppenheimer approximation is a relatively mild assumption and easily justifiable in many cases. In fact, it does not go too far in helping to solve more complicated problems, and even with this approximation there is only one molecular species that can be solved exactly: that of the Hydrogen-ion  $H_2^+$  which contains only one electron along with the two nuclei of the hydrogen atoms. However, from a conceptual point of view the approximation has some profound implications, such as the concept of the Potential Energy Surface (PES) which is defined by the electronic energy

over all possible nuclear coordinates. Other concepts such as equilibrium and transition state geometries are also born out of this approximation, since they are manifested through the PES. When electronic states are close in energy, the Born-Oppenheimer approximation often breaks down.

## 2.2 Wavefunction and Density Functional methods

### 2.2.1 Hartree-Fock and CASSCF

In this section, I will briefly explain the concepts behind the Hartree-Fock equations that form the basis for post-Hartree-Fock methods, such as the complete active space self-consistent field (CASSCF) method, which is extensively used in this thesis.

Adopting the Born-Oppenheimer approximation, the central problem left to solve in quantum chemistry is to find the ground and excited state energies of the electronic Hamiltonian for fixed nuclei. In 1928 a powerful approximation attempting to solve the ground state problem was proposed by Hartree [4] in what came to be known as the Hartree equations. The many particle wavefunction is represented as a product of  $N$  one-electron wavefunctions.

$$\Psi(r_1, \dots, r_N) = \prod_{i=1}^N \psi_i(r_i) \quad (2.7)$$

Here, the electronic spin and the Pauli exclusion principle, which states that two identical fermions cannot occupy the same quantum state simultaneously, were not taken into account. The Hartree wavefunction still assumed that the same spinorbital  $\psi_i(r_i)$  would not be occupied by more than one electron, but neglected quantum statistics and so the symmetry of the wavefunction was incorrect. To overcome the problem of the indistinguishability of electrons, Fock [5] and Slater [6] independently proposed a variational scheme for the total wavefunction that makes use of a determinant, the so-called Slater determinant. This determinant ensures that the wavefunction has the correct symmetry properties. Under an exchange of two particle indexes fermions require an anti-symmetric wavefunction, thus obeying the Pauli exclusion principle. A linear combination of different  $N$ -electron Slater determinants is also antisymmetric. The Slater determinant is written as:

$$\Psi_{HF} = \frac{1}{\sqrt{N!}} \begin{vmatrix} \psi_1(x_1) & \psi_1(x_2) & \cdots & \psi_1(x_N) \\ \psi_2(x_1) & \psi_2(x_2) & \cdots & \psi_2(x_N) \\ \vdots & \vdots & \ddots & \vdots \\ \psi_N(x_1) & \psi_N(x_2) & \cdots & \psi_N(x_N) \end{vmatrix}$$

The Hamiltonian operator, with consideration of the Born-Oppenheimer approximation, can be expressed as:

$$\hat{\mathcal{H}} = \hat{h} + \hat{g} + h_{NN} = \sum_{pq} h_{pq} E_{pq} + \frac{1}{2} \sum_{pqrs} g_{pqrs} e_{pqrs} + h_{NN} \quad (2.8)$$

Here  $\hat{h}$  and  $\hat{g}$  are mono-electronic and bio-electronic operators,  $E_{pq}$  and  $e_{pqrs}$  are the corresponding one and two-electron shift operators and  $h_{NN}$  is the nuclear-nuclear repulsion energy. If the bio-electronic contributions are neglected, an approximate wave function and associated eigenvalue for the Hamiltonian can be obtained by diagonalizing the mono-electronic part in a given one-electron basis, which may subsequently be used as a trial wave function. The Hartree-Fock method is a simple model that provides a wave function which considers bio-electronic interactions in an effective manner.

The Hartree-Fock one-electron orbitals are conveniently orthonormalized so that:

$$\langle \psi_i | \psi_j \rangle = \delta_{ij} \quad i, j = 1, \dots, N$$

The one-electron wavefunctions can be expanded as products of spatial functions  $\phi(r)$  and spin functions  $\sigma(s)$ , and are thus known as spin-orbitals. An initial guess of functions is used to form a Slater determinant and then the goal is to seek the Slater determinant that minimizes the energy expectation value. For each spin-orbital we will be solving an equation of the form:

$$\hat{F} \psi_i = \epsilon_i \psi_i \quad i = 1, \dots, N \quad (2.9)$$

which are the canonical Hartree-Fock equations.  $\hat{F}$  is the Fock operator and comprises of the following terms:

$$\hat{F} = f + \sum_{j=1}^n (J_j - K_j) \quad (2.10)$$

The first term on the right hand side of Equation 2.10 contains the one electron operators consisting of the electron kinetic operator and the potential operator between electrons and the nucleus. The  $J_j$  and  $K_j$  terms are operators that contain information of the 2-electron integrals, the Coulomb potential between electrons and the so-called 'Exchange' integral, respectively. The Exchange energy arises due to the Pauli principle and is a purely quantum mechanical contribution. They are defined:

$$\langle \psi_k \psi_j | \frac{1}{r_{12}} | \psi_i \psi_j \rangle = \langle \psi_k | J_j | \psi_i \rangle \quad (2.11)$$

$$\langle \psi_k \psi_j | \frac{1}{r_{12}} | \psi_j \psi_i \rangle = \langle \psi_k | K_j | \psi_i \rangle \quad (2.12)$$

Thus the solutions to the Hartree-Fock equations can be acquired by solving for the eigenfunctions  $\psi_j$  upon which  $\hat{F}$  depends. These equations are solved iteratively until we arrive at a self-consistent solution, therefore the Hartree-Fock method is also known as the self-consistent field (SCF) method.

A physical interpretation of the Hartree-Fock method is that each electron moves in a potential which is due to the nuclei and the average of the potential of all other electrons. This means that all other electronic spin-orbitals must be known when computing the one-electron wavefunction. Therefore, an approximate starting set of spin-orbitals are usually used and then the Hartree-Fock equations are applied to calculate the matrix elements of the Fock operator, diagonalizing it and obtaining a set of new orbitals. The total energy is then calculated and the new orbitals are used to calculate a new Fock operator and the process repeated iteratively until the energy converges to a precision that lies within a given threshold. Therefore, the underlying problem is to search a global minimum of the energy functional  $\langle \Psi | \hat{H} | \Psi \rangle$  with the constraint that the wavefunction be represented as a Slater determinant of one-electron spin-orbitals.

A major short-coming of the Hartree-Fock method is what is known as *correlation energy*. It does not consider instantaneous Coulombic interactions between electrons. It neglects certain correlation effects on electron distributions because it treats the effects of the  $N - 1$  electrons on the electron of interest in an average way. We deal with these short comings by making use of the so-called post-Hartree-Fock methods, which improve upon the Hartree-Fock method by including electron correlation and are thus a more accurate way of including repulsion between electrons, rather than treat them in an average way. In the Configuration Interaction (CI) method, possible  $N$ -electron Slater determinants (generated in the given basis set) are used as basis themselves, so that the exact ground-state or excited-state wavefunctions can be expressed as linear combinations of all possible  $N$ -electron Slater determinants:

$$\Psi = C_o \Phi_{HF} + \sum C_a^p \Phi_a^p + \sum C_{ab}^{pq} \Phi_{ab}^{pq} + \sum C_{abc}^{pqr} \Phi_{abc}^{pqr} + \dots \quad (2.13)$$

Any equation of this form is known as CI [7]. The first term is the Hartree-Fock term and the difference between the Hartree-Fock limit and the exact non-relativistic energy of the full-CI is called the correlation energy. If we work with a complete basis set, then the solution will be exact (for a given Hamiltonian). For computational efficiency the series of determinants may be

truncated to contain excitations upto a given level (single, doubly etc. excited configurations). Whereas in CI, only the coefficients in Equation 2.13 are optimized, in the multiconfiguration self-consistent field method(MCSCF) the orbital coefficients, along with the expansion coefficients  $C_i^j$  from Equation 2.13 are optimized simultaneously. One scheme of the MCSCF method is the complete active-space self-consistent field method(CASSCF) [8] where spin-orbitals are divided into inactive orbitals that are usually the lowest energy spin-orbitals and doubly occupied, virtual orbitals that are normally high energy unoccupied spin-orbitals and the active orbitals in which the orbital occupation varies in different determinants. After an initial SCF (HF) calculation is performed to determine orbitals, a full-CI wavefunction is calculated within the active space by taking all possible permutations of the electrons across the various orbitals (obeying the basic quantum mechanical laws of course).

CASSCF is an elegant method that deals with the multiconfigurational character of electronic states, limiting the CI expansion and can also be considered size-extensive (where size-extensivity is a mathematically formal characteristic referring to the linear scaling of a method with the number of electrons). In CASSCF the orbitals are split into three categories: (1) the inactive space, in which orbitals are doubly occupied, (2) the active space, which can have all possible configurations of electrons and (3) the virtual space that are always unoccupied. What is desirable, of course, is that we include a large number of orbitals within the active space but due to computational constraints one must choose a limited choice of orbitals within the active space. A particular difficulty arises when the number of electrons is equal to the number of active orbitals, since the permutations to arrange active electrons will be highest. In this thesis for the calculations involving Gadolinium(III) we consider 7 electrons over 7 active orbitals. The CASSCF wavefunction serves as a reasonable reference state to recover a larger fraction of correlation energy, in the multi-reference configuration interaction (MRCI) and n-electron valence state perturbation theory (NEVPT2) methods.

### 2.2.2 Density Functional Theory

Most of the wave-function based methods are an extension of the Hartree-Fock equations in one form or another. As we reach larger systems with large basis sets, the computational effort of calculations is increased, often exponentially even though nowadays there are near-linear scaling approximate algorithms. An alternative method was developed for solving a many-body interacting system utilizing its electronic probability density, which also takes into account

electron correlation. This sort of method is in principle exact and very effective, since only the density is required to derive the energy but in practice orbitals are used in all practical approximations and hence the scaling is comparable to Hartree-Fock, more or less, depending on the choice of functional. Density Functional Theory does not rely on knowledge of the wave function, which may be an extremely complicated function of electronic spatial and spin coordinates, but instead relies solely on the total one-electron density:

$$\rho(r) = N \int \dots \int |\Psi(\mathbf{x}_1, \mathbf{x}_2, \dots, \mathbf{x}_N)|^2 d\sigma d\mathbf{x}_2 \dots d\mathbf{x}_N \quad (2.14)$$

Since it is based on the electronic density it came to be known as Density Functional Theory (DFT). The foundational pillars of DFT were first put forth by Kohn and Hohenberg during the 1960's [9]. The theorems described in the paper show that, given the exact density functionals, one can find the exact ground-state density and energy of an  $N$ -electron system in an external scalar potential using the total density as variational objects. The Hohenberg-Kohn theorem can be summarized in two statements: (i) The external potential  $V_{ext}(r)$  is a unique functional of the electron density  $\rho(r)$ , (ii) The electron density  $\rho(r)$  that minimizes the energy is that of the ground state,  $\rho_0(r)$ . Because of its computational efficiency and relatively agreeable accuracy for larger systems, DFT has come to dominate many aspects of quantum chemistry, chemical physics, molecular physics, solid-state science, computational physics and condensed matter systems.

The roots of DFT can be traced back to 1927, when Thomas and Fermi proposed a density functional derived from a non-interacting uniform electron gas [10] [11]. In other words atoms would be described as uniformly distributed electrons (a negatively charged cloud) around nuclei in six-dimensional phase space (consisting of momenta and coordinates).

$$E_{TF}[\rho] = T_{TF}[\rho] + J[\rho] \quad (2.15)$$

Here the first term on the right hand side,  $T_{TF}[\rho]$  is the kinetic energy functional, which is also referred to as a Local Density Approximation (LDA), while the second term contains the electron-nucleus attraction and the electron-electron repulsion, often accounted for in a Hartree-Fock like manner by ignoring the self-interacting density.

$$T_{TF}[\rho] = 2.871 \int \rho^{5/3}(r) dr \quad (2.16)$$

$$J[\rho] = -Z \int \frac{\rho(r)}{r} d^3r + \frac{1}{2} \int \int \frac{\rho(r_1)\rho(r_2)}{r_{12}} dr_1 dr_2 \quad (2.17)$$

where  $Z$  is the nuclear charge. Paul Dirac in 1930 revised the Thomas-Fermi functional by accounting for the exchange Fermi-hole [12] by adding the term  $K_D = 0.74 \int \rho^{4/3}(r) dr$  to Equation 2.15.

Both these approximations are rather crude even though they have been used to study potential fields and charge density in metals and the equation of states of elements [13]. The approximation fails due to the poor description of the kinetic energy functional, and an improvement of this method is DFT. Considering a fully interacting system, the exact functional retains the true kinetic energy and electron-electron repulsions. If we consider non-interacting electrons, that simplifies the form of the functional to only a non-interacting kinetic energy functional, which if we employ orbitals ( $\phi_i$ ) (the so-called Kohn-Sham orbitals) can be written as:

$$T_{KS} = \min \sum_i \langle \phi_i | -\frac{1}{2} \nabla^2 | \phi_i \rangle \quad \text{where } \rho(r) = \sum_i |\phi_i(r)|^2 \quad (2.18)$$

The exact kinetic energy functional can thus be obtained, which is a lower bound to the one of the interacting system. Alongside this definition of the kinetic energy functional one may incorporate additional effects to the interacting systems. Those terms would be the kinetic-energy correlation correction  $T[\rho] - T_{KS}[\rho]$  and the bielectronic exchange-correlation (XC) correction, whose sum provides us with the well-known exchange-correlation functional,  $E_{XC}[\rho]$ .

Very simply put DFT provides an exact energy correspondence for the many-electron wave function from knowledge of just the electron density. The ground state energy associated with the density is available through the functional.

$$E[\rho] = \int \rho(r) V_{ext} dr + F[\rho] \quad (2.19)$$

In orbital free DFT the kinetic energy can be approximated in terms of the density, (orbital free DFT could in principle be exact, but no one has found the universal functional yet) for example by making use of the Thomas-Fermi model [10] [11]. In 1965 Kohn and Sham derived a set of one-electron equations from which the electron density could be obtained [14]. By using electron orbitals we get a better approximation of the kinetic energy for the density functional. Using the Kohn-Sham orbitals, Kohn and Sham showed that the exact ground state energy can be written as:

$$E[\rho] = -\frac{1}{2} \sum_i \langle \phi_i | \nabla_i^2 | \phi_i \rangle + \int \rho(r) V_{ext} d^3 r + E_{coulomb}[\rho] + E_{xc}[\rho] \quad (2.20)$$

which consists of electron kinetic energy, electron-nuclear attraction and coulomb contributions respectively. Since the coulomb potential energy does

not include contributions due to exchange-correlation effects, an additional exchange correlation term must be added to the total energy contribution  $E_{xc}$ .

The use of multi-determinantal wave function based methods results in an exponential increase in calculations with each additional particle, but using the occupied orbitals or fictitious one-electron wavefunctions the number of equations to compute is drastically decreased. For example to represent one electron in a mesh of 10 points each along the x, y and z axis would require  $10^3$  numbers, but a 17 electron system would require  $10^{51}$  numbers for a correlated wavefunction. An orbital description would require only  $17 \times 10^3$  numbers to compute, which is a much simpler problem to solve. The main problem with DFT methods is that the exact functional is unknown and a lot of approximate XC-functionals have been developed. There is no *a priori* way to determine which functionals may benefit which calculations and usually with time one is able to say that a particular functional works for calculating a particular property of a complex, but it is only with empirical experience that DFT methods seem to be the most successful.

## 2.3 Relativistic Quantum Mechanics

Although the Schrödinger equation is capable of describing many phenomena, it does not take relativistic effects into account. Relativistic effects can effect orbital sizes and shapes, and hence interaction energies and molecular properties, and become increasingly important for heavier atoms, where the electrons begin to obtain relativistic speeds. In this thesis we are interested in the Zero-Field-Splitting, which is influenced by spin-orbit coupling, a relativistic effect. Zero-Field Splitting is the splitting of degenerate energy levels of an open-shell ground state in the absence of an external magnetic field. Here degeneracy simply means that pairs of electrons in the active orbitals all occupy the same energy levels. In the presence of a magnetic field these can be split by an effect known as the Zeeman effect. However, due to relativistic effects, the degeneracy can be split and since there is zero magnetic field this splitting came to be known as Zero-Field Splitting (ZFS). There are several ways that relativistic calculations can be performed and here I present two of the most common methodologies that are used today and were used in our studies: the Zeroth-Order Regular Approximation (ZORA) [15][16] and the Douglas-Kroll-Hess (DKH) approximation[17] [18].

### 2.3.1 The Dirac Equation

Under Einstein's theory of special relativity all physical laws must be invariant under Lorentz transformation. This condition is not fulfilled by the Schrödinger Equation since temporal and spatial derivatives appear in non-symmetric form. Paul Dirac was the first to combine the wave mechanics of Schrödinger and the theory of special relativity and was able to deduce a formula that fulfilled both conditions [19]. This symmetric treatment of time and space is fulfilled by the Dirac Hamiltonian:

$$H_D = c\alpha \cdot p + (\beta - 1)mc^2 + V \quad (2.21)$$

Here  $\alpha$  is a 3-vector whose elements  $\alpha_k$  consist of  $4 \times 4$  matrices,

$$\alpha_k = \begin{pmatrix} 0 & \sigma_k \\ \sigma_k & 0 \end{pmatrix}, \quad k = x, y, z \quad (2.22)$$

where  $\sigma_k$  are the Pauli spin matrices, and  $\beta$  is a diagonal matrix with entries (1, 1, -1, -1). Equation 2.21 is the starting point of all molecular relativistic calculations and may be reformulated as two coupled differential equations for the two spinor components.

$$\begin{pmatrix} V(r) - E & c(\sigma \cdot p) \\ c(\sigma \cdot p) & V(r) - E - 2mc^2 \end{pmatrix} \begin{pmatrix} \Psi^L(r) \\ \Psi^S(r) \end{pmatrix} = 0 \quad (2.23)$$

Since the Dirac equation is only valid for a one-electron system, the one-electron Dirac Hamiltonian has to be extended to a many-electron Hamiltonian to treat the chemically interesting many-electron systems.

### 2.3.2 ZORA approximation

An elegant approach by making use of elimination procedures to the four-component Dirac equation was proposed by Chang *et al.* [20] as well as Heully *et al.* [21] and later developed into a computational algorithm by the Amsterdam group [16]. This came to be known as the Zeroth-Order Regular Approximation (ZORA). By writing out Equation 2.23 in terms of two 2-component equations:

$$V\Psi^L + c\sigma \cdot p\Psi^S = E\Psi^L \quad (2.24)$$

$$c\sigma \cdot p\Psi^L + (V - 2mc^2)\Psi^S = E\Psi^S \quad (2.25)$$

we can use Equation 2.25 to describe  $\Psi^S$  in terms of  $\Psi^L$ :

$$\Psi^S = \left( \frac{c\sigma \cdot p}{E - V + 2mc^2} \right) \Psi^L \quad (2.26)$$

and substituting back into Equation 2.24 reveals,

$$V\Psi^L + \frac{1}{2}\sigma \cdot pK\sigma \cdot p\Psi^L = E\Psi^L \quad (2.27)$$

where

$$K = \left(1 + \frac{E - V}{2mc^2}\right)^{-1} \quad (2.28)$$

The regular approximation takes this value of  $K$  and expands it into a power series, which is the starting point for calculations.

$$K = \left(1 + \frac{E - V}{2mc^2}\right)^{-1} = 2c^2(2mc^2 - V)^{-1} - 2c^3E(mc^2 - V)^{-2} + \dots \quad (2.29)$$

By just including the first term of this expansion we get the Zeroth Order Regular Approximation.

$$H_{ZORA} = V + \sigma \cdot p \frac{c^2}{2mc^2 - V} \sigma \cdot p \quad (2.30)$$

The inclusion of the second term is called the First Order Regular Approximation (FORA), but the one-electron ZORA Hamiltonian is already a reliable relativistic correction. The mass-velocity correction as well as part of the Darwin term are missing from ZORA, and since the missing term is positive for bound states, ZORA results in energies that are too low. However, since it is bounded from below it makes the method variationally stable.

### 2.3.3 DKH approximation

The Dirac Hamiltonian from Equation 2.23 can be block-diagonalized with a suitable unitary operator  $U$ :

$$UH_DU^\dagger = \begin{pmatrix} H_+ & 0 \\ 0 & H_- \end{pmatrix} \quad (2.31)$$

$H_+$  and  $H_-$  are the positive and negative energy values of the full Dirac spectrum respectively, and the two-component equation can be written in terms of the positive energy solutions:

$$H_+\Phi = E\Phi \quad (2.32)$$

Douglas and Kroll noted in the appendix of their paper on the fine structure of helium [17] a possible scheme to carry out sequential unitary decoupling transformations. The method they suggested used the external potential  $V$  to classify contributions to  $H_+$ . This appendix note was not utilized

by quantum chemists until it was discovered by Hess [18] who sought its practical implementation by making use of the upper component of the Dirac eigenvector. The unitary transformation can be represented as a sequence of simpler unitary transformations:

$$U = \cdots U_3 U_2 U_1 U_0 \quad (2.33)$$

The unitary matrices  $U_m$  are chosen so that off-diagonal terms from the Dirac Hamiltonian vanish step by step and this procedure leads to even terms  $H$  and odd terms  $\mathcal{O}$ , and if a complete decoupling is achieved than the odd terms vanish and we will be left with a completely block-diagonal Hamiltonian. Furthermore, the  $H_+$  and  $H_-$  operators may be categorized into spin-free( $H^f$ ) and spin-dependent( $H^d$ ) parts. By truncating Equation 2.33 to a pre-defined order in the external potential  $V$ , the order of the scheme is defined.

## 2.4 ZFS and the Spin Hamiltonian formalism in Gd(III) complexes

To compute the ZFS several methods have been developed both in DFT and post-Hartree-Fock method. The standard KS-DFT implementations are unable to handle the multi-determinantal character of the spin eigenfunctions involved in the ZFS, hence most methodologies do not directly calculate the low-lying spin-orbit spectrum but evaluate the ZFS tensor to reconstruct the model spectrum *a posteriori*. In wave-function methods there are several ways to compute the ZFS. By using the Hartree-Fock method the multideterminantal character of the ground state is not well described and an important portion of the electron correlation is omitted. The ZFS computation proceeds in two steps: (i) a set of spin-orbit free states is computed at the CASSCF level (ii) low-lying spin-orbit spectrum can be computed directly through a state interaction (SI) method, which is used in this thesis.

To investigate ZFS one can invoke the spin Hamiltonian formalism upto second-order in the principal axis frame, which is parametrized with the cylindrical  $D$  and rhombic  $E$  parameters:

$$\hat{H}_{ZFS}^{(P)} = D[\hat{S}_z^2 - \frac{1}{2}S(S+1)] + E[\hat{S}_x^2 - \hat{S}_y^2]. \quad (2.34)$$

The ZFS term may be represented as a matrix in Hilbert space spanned by the  $|S, M_s\rangle$  kets and in the case of Gd(III), since  $S=7/2$  the dimensionality of the matrix will be 8. The matrix will be represented in terms of the two parameters  $D$  and  $E$ , which are related to the principal components of  $D$  in the principal axes frame:

$$D = D_{zz}^{(P)} - \frac{1}{2}(D_{xx}^{(P)} + D_{yy}^{(P)}),$$

$$E = \frac{1}{2}(D_{xx}^{(P)} - D_{yy}^{(P)}).$$
(2.35)

The full matrix is depicted in Figure 2.1b. For axial symmetry (no rhombic distortions), the rhombic parameter,  $E$ , is zero and as a consequence  $D_{xx} = D_{yy}$ . Therefore, neglecting rhombic contributions, one can express the energies of the Kramer doublets in Gd(III) compounds solely in terms of the ZFS parameter,  $D$ . The energy levels of the ground octet state will then be split in accordance to Figure 2.1a. However, in practical quantum chemical calculations the energies of the Kramer doublet might deviate from the relationships formulated in Figure 2.1a. This shows the limitation of the second order formulation of the spin-Hamiltonian.

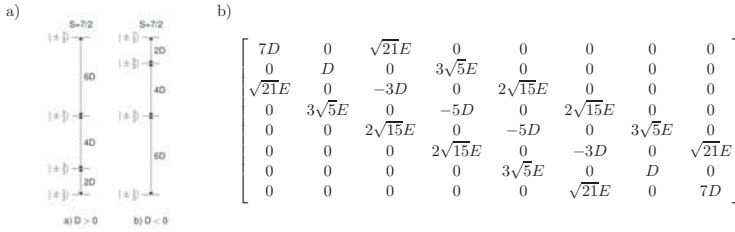


**Figure 2.1:** a) The ZFS of the Kramer doublets in symmetrical Gd(III) compounds (also applies for the isoelectronic Eu(II) metal center) expressed in the cylindrical  $D$  parameters. When the rhombic  $E$  parameter is included, the graphical representation does not apply. b) Relationship between  $D$  and  $E$  parameter in the full second order ZFS and the SI-matrix of the four Kramer doublets of the octet state

In the work related to Gd(III) complexes we consider an active space of 7 electrons included in the 7  $f$ -orbitals(14 spin-orbitals). In the given active space there are 1 octet, 48 sextets, 392 quartets and 784 doublet states, generating altogether  $\binom{14}{7}$  electronic states. However, for most of our calculations we only consider including the ground octet state and the sextet states. This is because the inclusion of the extra quartet and doublet states does not significantly effect the ZFS and is computationally demanding to perform.



# 3. Nuclear Magnetic Resonance and Spin Relaxation

## 3.1 Contrast agents for MRI scans

The physical principles behind magnetic resonance imaging (MRI) are based upon nuclear magnetic resonance (NMR) spectroscopy. MRI is a medical scanning technique which allows one to probe the structure of tissues in the body. It is a non-invasive technique which makes it especially suitable for clinical use, as compared to other scanning methods such as X-ray scans etc. NMR was discovered by Felix Bloch and Edward Purcell in 1946 [22; 23] for which they were awarded the Nobel Prize in Physics just a few years later in 1952 "for their discovery of new methods for nuclear magnetic precision measurements and discoveries in connection therewith". In the human body, it was found first in 1971 by Raymond Damadian that tumor tissues have longer NMR relaxation times as opposed to normal tissues [24] and Lauterbur and Mansfield were awarded the Nobel Prize in Medicine in 2003 for inventing the MRI. Richard Ernst suggested the use of phase and frequency encoding and Fourier transform which forms the basis of MRI scans used today [25].

MRI contrast agents are chemical complexes that increase the contrast between healthy and diseased tissues, thereby increasing accuracy and sensitivity of MRI scans. The contrast is created due to non-uniform decrease of relaxation times (discussed later) of proton spins in tissue by means of the fluctuating magnetic interaction with the electron spins of magnetic contrast media. One type of commonly used MRI contrast agents in practice are stable complexes of the paramagnetic metal ions containing Gd(III) at the core of the complex. Gd(III) contrast agents provide bright contrast in  $T_1$ -weighted images and are thus considered beneficial for such purposes. The class of  $T_2$  negative agents are usually based on iron-oxide particles.

Gadolinium based MRI contrast agents contain a central paramagnetic Gd(III) ion, a chelating ligand and consist of an inner sphere that usually contains one or two water molecules. The choice of Gd(III) as a contrast agent is due to two major reasons: (i) Gd(III) has a half-filled  $7f$  shell

containing 7 unpaired electrons and thus has a high magnetic moment (ii) Gd(III) has a symmetric  $S$  state which leads to relatively long electron spin relaxation times which leads to enhanced paramagnetic relaxation enhancement (discussed below). The first of the points above is obvious, but there are other ions such as Dysprosium(II) with higher magnetic moments, but the asymmetry of these electronic states leads to very rapid electron spin relaxation, and therefore this subtle difference makes Gd(III) suitable as a contrast agent. Furthermore, the water molecule that is coordinated within the inner sphere of the complex is also crucial since its nuclear spin is strongly influenced by the magnetic moment of the central paramagnetic ion.

**Table 3.1:** Some Gd(III) contrast agents used for medical scans, and their respective brand names and companies. These contrast agents are studied in this thesis.

Complex	Brand name	Company
Gd(III)HPDO3A(H <sub>2</sub> O)	ProHance	Bracco
Gd(III)DOTA(H <sub>2</sub> O) <sup>-</sup>	Dotarem	Guerbet
Gd(III)DTPA(H <sub>2</sub> O) <sup>2-</sup>	Magnevist	Schering

## 3.2 Basic physics behind NMR

Nuclear Magnetic Resonance(NMR) spectroscopy is an important tool to determine the structure and properties of atoms and molecules by observing the interaction of constituent nuclear spins of a sample with an external magnetic field. Each nucleus has an intrinsic spin quantum number  $I$  determined by the number of unpaired neutrons and protons, and is associated with  $2I+1$  energy levels, corresponding to each different magnetic quantum number  $m_I$  (where  $m_I = -I, -I+1, \dots, I-1, I$ ). These energy levels are degenerate in the absence of an external magnetic field, but when a magnetic field is applied they lose their degeneracy, an effect known as the Zeeman effect. In an applied magnetic field  $B_0$  the energy for a given spin state  $m_I$  is given by:

$$E_{m_I} = -\hbar m_I \gamma B_0 \quad (3.1)$$

where  $\gamma$ , the gyromagnetic ratio of an isotope, is the ratio of its magnetic dipole moment to its angular momentum and is unique for each nucleus. The difference in energy between two consecutive energy levels is given by:

$$\Delta E = \hbar \gamma B_0 = h \omega_0 \quad (3.2)$$

The resonance frequency  $\omega_0$  is known as the Larmor frequency and is therefore:

$$\omega_0 = \frac{\gamma B_0}{2\pi} \quad (3.3)$$

The populations of energy levels  $n_i$  for an  $N$  spin system can be written as Boltzmann distributions and the ratio of populations can be expressed as:

$$\frac{n_a}{n_b} = \exp\left(-\frac{\Delta E}{k_B T}\right) \quad (3.4)$$

The population difference is directly proportional to the intensity of NMR signals and therefore, high magnetic fields and low temperatures result in more intense resonances. The chemical shift( $\delta$ ) represents the difference in resonance positions of an observed sample and a reference sample. The interaction is caused by electrons in the vicinity of a nucleus, and shifts the Zeeman energy levels influencing the frequency of transition between levels.

### 3.3 Nuclear Spin Relaxation

The concept of relaxation invokes the image that the system under considerations is being perturbed, and relaxes back into an equilibrium state. In NMR spectroscopy this perturbation may be attributed to a radiofrequency pulse. When molecules absorb an electromagnetic pulse they are transferred from lower energy states to higher energy states. Light in the radio-frequency range cause spins to 'flip' or jump to higher energy states. Then, relaxation is the process by which spins return to an equilibrium configuration. This equilibrium configuration can be described as the state where the populations of energy levels follow a Boltzmann distribution and where no coherences are present in the system. Relaxation can be described in terms of two relaxation times:  $T_1$ , the spin-lattice, and  $T_2$ , the spin-spin relaxation. Spin-lattice relaxation refers to the component of the magnetization vector along the applied magnetic field (the 'spin') reaching equilibrium with its surroundings (the 'lattice'). Spin-lattice relaxation is a first order kinetic process:

$$\frac{dM_z}{dt} = -\frac{M_z - M_0}{T_1} \quad (3.5)$$

where  $M_0$  is the equilibrium magnetization and  $M_z$  is the magnetization at time  $t$ :

$$M_z = M_0 e^{-\frac{t}{T_1}} \quad (3.6)$$

For the energy transfer to occur the motion of the lattice must cause a fluctuating magnetic field at the site of the spin involved, and only the  $x$  and

the  $y$  components of the local field can cause  $T_1$  relaxation.

On the other hand, spin-spin relaxation is the exponential decay of the transverse component of the magnetization vector  $M_{xy}$ . It takes the form:

$$M_{xy} = M_{xy,0} e^{-\frac{t}{T_2}} \quad (3.7)$$

where  $M_{xy,0}$  is the initial value of the transverse magnetization and  $M_{xy}$  is the transverse component of magnetization at time  $t$ . Under perturbation the decay of the signal in the  $xy$ -plane is faster than the decay of the magnetization along the  $z$ -axis. This decay is due to the loss of phase coherence of the microscopic components, which is partially caused by the differences in the Larmor frequencies induced by the applied magnetic field at different locations in the sample. It is also caused by chemical exchange, which can lead to line broadening, an important tool for the measurement of relaxation rates. In the next sections I will briefly look at some of the mechanisms that drive relaxation. Thereafter, I give a brief section on how molecular dynamics and quantum chemical calculations can assist in understanding the relaxation process in NMR.

### 3.3.1 Dipole-Dipole Interactions

Each spin has a magnetic moment which gives rise to a local magnetic field which can interact with other spins. This mechanism is therefore, due to two spins, one that generates the magnetic moment, and the other that experiences it. The size of the interaction between two spins is proportional to the inverse cube of the distance between them (the interaction falls quickly as  $(\frac{1}{r^3})$ ) and the product of the gyromagnetic ratios of the two nuclei involved; it is dependent on the magnetic dipoles of the two spins  $\mu_I$  and  $\mu_S$ . Furthermore the orientation of the vector joining the two spins relative to magnetic field also influences the dipolar mechanism.

$$E_{dd} = \frac{\mu_I \cdot \mu_S}{r_{IS}^3} - \frac{(\mu_I \cdot r_{IS})(\mu_S \cdot r_{IS})}{r_{IS}^5} \quad (3.8)$$

Here  $\mu_I = \hbar\gamma_I I$  and  $\mu_S = \hbar\gamma_S S$ . Dipole interaction provides a path by which energy can be transferred from the spin to the lattice. Dipole-dipole interaction turns molecular motion into an oscillating magnetic field which causes spin transitions. The relaxation is caused if the fluctuations occur at the Larmor precession frequency. The correlation time for dipole-dipole relaxation is governed by molecular motion.

### 3.3.2 Chemical Shift Anisotropy

Two interactions are discussed here that affect the relaxation mechanism: chemical shift anisotropy (CSA) and quadrupolar relaxation. Chemical shifts reflect the electronic environments that modify the local magnetic fields experienced by different nuclei. Electrons in a molecule may induce local fields at the nucleus. The Larmor frequency is therefore shifted, since it experiences the sum of the applied and induced field. These chemical shifts may provide structural information. The precession frequency is written as:

$$\omega = -\gamma(1 - \phi)B_0 \quad (3.9)$$

$\phi$  is a dimensionless quantity depicting the isotropic nuclear shielding. The chemical shift is defined in terms of the NMR frequency of a given resonance and a reference sample:

$$\delta_{sample} = \frac{\omega_{sample} - \omega_{ref}}{\omega_{ref}} = \frac{\phi_{ref} - \phi_{sample}}{1 - \phi_{ref}} \quad (3.10)$$

Chemical shielding is described by a chemical shift tensor, which transforms the static field into an effective field. Due to these shielding effects the effective field  $B_{eff}$  may deviate from the direction of the static field  $B_0$ . Because of the rapid rotation of the molecule in solution the observed chemical shift is an average over the shifts corresponding to the different orientations. The magnetic field experienced by the nucleus depends on the orientation of the molecule relative to the applied magnetic field. This phenomenon is termed CSA.

Nuclei with spin angular momentum  $I > 1/2$  are characterized by an additional mechanism for relaxation, the quadrupolar interaction which arises due to the non-spherical distribution of charge in the nucleus. These nuclei have an electric quadrupole moment  $Q$  which interacts with the electric field gradient present at the nucleus, and the interaction is anisotropic (it depends upon orientation). The high efficiency of quadrupolar relaxation is associated with the large strength of the quadrupolar coupling constant which in certain cases may be magnitudes larger than the dipolar coupling constant.

## 3.4 Paramagnetic effects in NMR

### 3.4.1 Paramagnetic Relaxation Enhancement

Paramagnetic species contribute strongly to the nuclear spin relaxation which is why they have garnered significant interest. In systems that contain a

paramagnetic central ion, this enhancement is due to the large magnetic moment associated with unpaired electron spins around the metal center. The dipole-dipole interaction between the nuclear spin  $I$  and electron spin  $S$ , generally dominate the effects.  $^{17}\text{O}$  is an exception to this rule where the scalar interactions of the hyperfine interaction are the primary contributors. When dealing with paramagnetic relaxation enhancement we must consider two cases, the inner-sphere relaxation, where the nuclear spin resides in the first co-ordination sphere of the paramagnetic ion, and the outer sphere relaxation. Luz and Meiboom [26] showed that the PRE in the inner-sphere longitudinal relaxation is related to the solution composition, exchange lifetime and the in-complex relaxation rate.

The Paramagnetic Enhancement effect in Gd(III) is large, owing to the large magnetic moment of the 7 unpaired electron and relative slow electron spin relaxation, which makes it suitable for larger systems at distances of up to 35 Å. Paramagnetic Relaxation Enhancement can be manifested through direct dipole-dipole interactions or through Curie-Spin Interactions. The Curie-Spin Relaxation arises from dipole-dipole interaction between a nucleus and the time-averaged magnetization of the electrons.

### 3.4.2 Pseudocontact Shift

The electron magnetic moment is usually treated by its isotropic spin contribution and its anisotropic orbital contribution. When the orbital contribution is large the induced magnetic moment shifts in intensity, inducing an anisotropic change in the magnetic susceptibility tensor. The net contribution by the dipole interaction in this case does not equal zero, and there will be a shift in the external magnetic field which is termed the pseudocontact shift  $\delta_{PCS}$ . The shift is caused by the dipolar interaction between magnetic moments of the nucleus and unpaired electrons. The theoretical framework to describe the relationship between pseudocontact shift and dynamics is still an active area of research and has not been fully established yet.

### 3.4.3 Residual Dipolar Couplings

The partial orientation of molecules result in incomplete rotational averaging of the dipolar and quadrupolar couplings which causes splittings in the NMR spectra. These incompletely averaged dipolar couplings are termed Residual Dipolar Couplings (RDC) and provide a source for structural information by defining long-range ordering in a molecule [27] [28]. RDC generated by paramagnetic alignment with the external magnetic field allow unique opportunities to probe conformational variation.

### 3.5 Electron spin relaxation parameters from First-Principle Molecular Dynamics

Having discussed the general methodologies used in quantum chemistry in Chapter 2, it is now time to relate some of the ideas discussed to the parameters that are produced from NMR relaxation experiments. When speaking about the dynamics in solution we are particularly interested in those mechanisms that will affect the relaxation times  $T_1$  and  $T_2$ , the spin-lattice and spin-spin relaxation times explained in the relaxation section. Being a dynamic process, to have direct correspondence with experiment, one must resort to dynamical simulations such as Molecular Dynamics (MD). There are several ways in which these kinds of simulations can help when comparing to experimental data. Correlation times for translational, angular rotational and re-orientational motions are some of the components that can be extracted from MD simulations and related to relaxation theories.

Furthermore, from the MD simulations one is able not only to extract correlation times, but indeed correlation functions which can provide deeper insight into molecular motions and interactions. In general, the rotational diffusion or tumbling is an extremely important dynamic mechanism in NMR spectroscopy. The proton relaxation can for example arise from the rotational motion of a rigid molecule. Molecular dynamics simulations can directly explore the molecular rotational diffusion at picosecond and nanosecond time scales and are an extremely useful tool for this purpose. Vibrations are normally considered to contribute to the average coupling. Through molecular dynamics we can get insight into the internal vibrations, librations, rotations/re-orientations and translations of a molecular system.

The mechanisms thought to have been the most effective in reducing  $T_1$  were molecular tumbling and inner-sphere water exchange. However, the importance of electronic spin relaxation on the shortening of  $T_1$  that is caused by Gd(III) contrast agents has in recent years begun to catch the attention of scientists. Longer electronic relaxation  $T_{1e}$  allows strong hyperfine interactions between nuclear and electronic spins leading to faster  $^1\text{H}$  relaxation times. The electronic spin relaxation is caused by the effect of fluctuations of the zero-field splitting (ZFS) spin Hamiltonian in the laboratory frame. The ZFS is the result of electron repulsion, spin-orbit coupling and the effect of the ligand field on the ground state. The overall ZFS will be dependent on the orientation of the complex and its instantaneous conformation in the laboratory frame. Furthermore, one is to assume that amidst a mean equilibrium conformation of the compound the various components undergo vibration and libration around

the molecular frame to which it is rigidly bound. In this frame, the ZFS spin hamiltonian has a time average value which is time independent and therefore called the static ZFS. The difference,

$$\hat{\mathcal{H}}_{ZFS,Total}^{(M)}(t) - \hat{\mathcal{H}}_{ZFS,Static}^{(M)} = \hat{\mathcal{H}}_{ZFS,Transient}^{(M)}(t) \quad (3.11)$$

is called the transient ZFS. To obtain the time-dependent transient tensor one can subtract the static  $\bar{\bar{D}}_{static}$  tensor from each instantaneous  $\bar{\bar{D}}$ ,

$$\bar{\bar{D}}_{trans} = \begin{pmatrix} d_{11} & d_{12} & d_{13} \\ d_{21} & d_{22} & d_{23} \\ d_{31} & d_{32} & d_{33} \end{pmatrix} \quad (3.12)$$

Parameters extracted from the static and transient Hamiltonian can subsequently be used as a basis for describing both electronic and nuclear spin relaxation. For instance a simple expression for the longitudinal electron spin relaxation rate was proposed by Belorizky and Fries [29]:

$$\frac{1}{T_{1e}} = \frac{2}{5} \Delta_S^2 \tau_2 \left( \frac{1}{1 + \omega_0^2 \tau_2^2} + \frac{4}{1 + 4\omega_0^2 \tau_2^2} \right) + \frac{12}{5} \Delta_T^2 \tau_v \left( \frac{1}{1 + \omega_0^2 \tau_v^2} + \frac{1}{1 + \omega_0^2 \tau_v^2} \right) \quad (3.13)$$

which uses the magnitudes of the static( $\Delta_S$ ) ZFS which is defined by the static components used in Eq. 3.14.

$$\Delta_S = \sqrt{2/3 D_S^2 + 2 E_S^2} \quad (3.14)$$

On the other hand the transient( $\Delta_T$ ) contribution is originally introduced in the so-called pseudo-rotation model [30; 31]. The Brownian motion of the complex causes a time-dependent perturbation as the  $\bar{\bar{D}}_{static}^{(M)}$  tensor modulates the  $\hat{H}_{ZFS,static}^{(L)}$  by reorientation in the laboratory frame which is characterized by a rotational correlation time  $\tau_2$ , whereas  $\tau_v$  is the correlation time associated with the fluctuation of the transient ZFS in the molecular frame  $\bar{\bar{D}}_{trans}^{(M)}$ .  $\omega_0$  in Equation 3.14 is the electron spin Larmor frequency. Fast molecular re-orientation introduces stochastic time dependence on the electron nuclear dipole-dipole coupling interaction which effects the paramagnetic relaxation enhancement. In Paper II by using FPMD and CASSCF we compute the static ( $\Delta_S$ ) ZFS along with the correlation time of the transient ZFS  $\tau_v$  for a Gd(III) complex that is relevant as an MRI contrast agent, thereby providing an important piece of the puzzle in forming a more complete picture of the electron spin relaxation for this complex, furthermore pushing the boundaries of computationally accurate simulations to compare to experimental estimates.

## 4. Summary of Results

This chapter includes a summary of results derived from four papers, and is divided into four sections. The first section deals with simple symmetrical systems with quenched ZFS. The objective here is two-fold: first to detect the scale of error we are dealing with, and secondly to see the response of the ZFS when various systematic distortions are applied, thereby breaking the symmetry. In the second section I discuss some of the drawbacks of using DFT to calculate the static ZFS and compare values obtained from DFT and CASSCF calculations to experimental values. The third section discusses paramagnetic ions in water. In particular, I compare the iso-electronic aqueous Gd(III) and Eu(II) systems and find that there isn't a simple relationship between the two systems in spite of them having similar electronic structures (each having 7-*f* valence electrons). A discussion of the effects of the inclusion of an 'outer shell' in aqueous Gd(III) is also presented. The sizes of the inner and outer shells are determined by running MD simulations. Finally, in the fourth section I bring together first-principle molecular dynamics simulations and quantum chemical calculations to calculate the correlation time of the transient ZFS, for a Gd(III) system that is of clinical relevance, and find that it is on the sub-picosecond scale showing a faster decay than experimental estimates.

### 4.1 Symmetrical systems: $O_h$ and $T_h$ symmetry

#### 4.1.1 ZFS in symmetrical Gd(III) systems

We began by investigating the free Gd(III) ion. The purpose was to assess the scale of error we may expect in the ZFS calculations on Gadolinium(III) complexes. The free ion produced an artificial splitting of the ground state octet utilizing the CASSCF method, but this splitting is quenched and we were able to obtain a degenerate ground state when a further MRCI calculation on top of the CASSCF (known forthwith as CASSCF/MRCI0) was performed. We also tested for various convergence criteria and basis set dependence.

Using this CASSCF/MRCI0 method, we investigated two idealised Gadolinium(III) complexes:  $Gd(III)F_6^{3-}$  and  $Gd(III)(H_2O)_6^{3+}$  characterized by

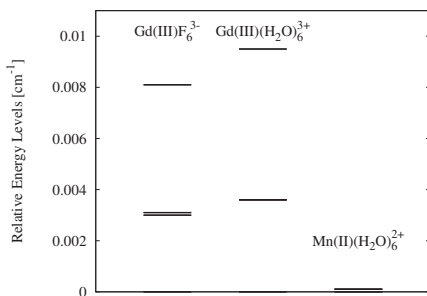


**Figure 4.1:** Comparison of the artificial ZFS of the Kramer Doublets in the Symmetrical Complexes

$O_h$  and  $T_h$  symmetry respectively. A third complex:  $Mn(II)(H_2O)_6^{2+}$  was also used to compare the ZFS response of  $S = 7/2$  systems to  $S = 5/2$  systems. The geometries were obtained using constrained optimization in order to preserve symmetry. Because of these symmetry constraints, we would expect there to be no splitting of the ground state in these complexes.

A comparison of the splitting of energy levels is shown in Figure 4.1 and we see that the octahedral complex  $Gd(III)F_6^{3-}$  has a slightly lower splitting than the hexa-aqua  $Gd(III)$  complex, of  $T_h$  symmetry. The ground state splitting of both complexes is less than  $0.01 \text{ cm}^{-1}$  which is quite small, although they should ideally be 0. The hexa-aqua  $Mn(II)$  system shows a degenerate energy level upto the precision recorded, and we only witnessed the artefact for heavy  $f$ -electron systems.

We chose to distort the complexes  $Gd(III)F_6^{3-}$ ,  $Gd(III)(H_2O)_6^{3+}$  and  $Mn(II)H_2O_6^{2+}$  along a single axis and see the effect of this axial distortion on the splitting of the Kramer doublets as depicted in Figure 4.2. The distortion has a larger effect on the splitting of  $Gd(III)F_6^{3-}$  as compared to the other two complexes. The response to distortion of the ZFS is of similar magnitude in the aqueous  $Gd(III)$  and  $Mn(II)$  complexes. It was found that the off-diagonal SOC elements in the SI matrix for  $Gd(III)$  complexes are an order of magnitude larger than for the  $Mn(II)$  complex and this may explain the similar magnitude, since the energy separation between the ground state and low lying excited state is much lower in energy for the hexaaqua  $Mn(II)$ .

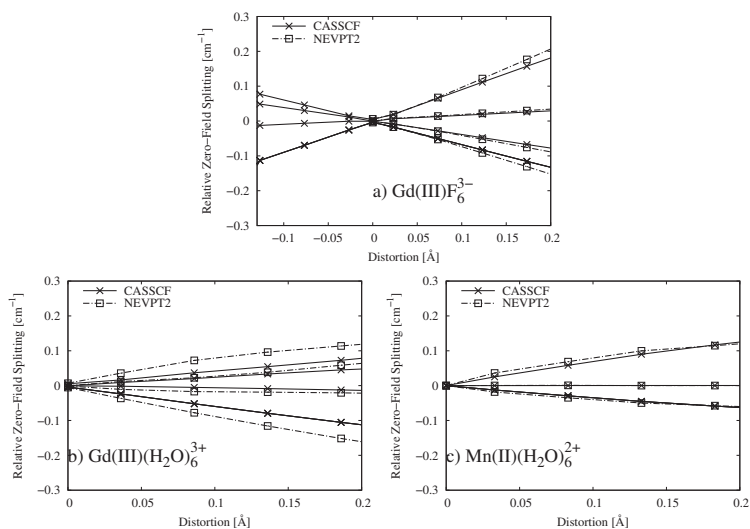


**Figure 4.2:** ZFS of Kramers Doublets under Axial Distortion of Gd(III)F<sub>6</sub><sup>3-</sup> in panel (a), of Gd(III)H<sub>2</sub>O<sub>6</sub><sup>3+</sup> in panel (b) and of Mn(II)H<sub>2</sub>O<sub>6</sub><sup>2+</sup> in panel (c). For the Gd(III)F<sub>6</sub><sup>3-</sup> complex, we have included CASSCF results for negative distortions, which shows that the curves are smooth and the ZFS *D* parameter changes sign while passing through the structure of *O<sub>h</sub>* symmetry. NEVPT2 results are shown as dashed lines.

#### 4.1.2 ZFS associated with vibrational motion of aqueous Ni(II) and Mn(II)

Multi-configurational quantum chemical calculations are employed to study how geometric fluctuations influence the zero-field splitting (ZFS) of paramagnetic ions in aqueous solution. The ZFS is calculated for systematic distortions from  $T_h$  symmetry of the hexa-aqua  $\text{Mn(II)(H}_2\text{O)}_6$  and  $\text{Ni(II)(H}_2\text{O)}_6$  complexes along all vibrational normal modes. In this way we are able to determine the distortion modes that have the strongest effect on the ZFS. The purpose of the study is to establish the structural mechanisms behind the ZFS fluctuations in aqueous Ni(II) and Mn(II) by analysis of the ZFS response as a function of the distortions of the metal hexa-aqua clusters. Thereby, we can establish a theoretical framework for decomposition of the instantaneous distortion in the idealized distortions along normal modes of the ground state vibrations of the hexaaqua complex from  $T_h$  symmetry. We explicitly show that only a few degrees of freedom contribute significantly to variations in the ZFS whereas due to symmetry the other modes remain dormant and the second-order spin Hamiltonian is not greatly affected by distortions of these modes. Among the 'active' modes the 2 degenerate  $E_g$  modes are decisive and display the largest amount of splitting. On top of that a few  $T_g$  and  $T_u$  modes of mixed character, which include distortions of the  $\text{MO}_6$  unit along with HOH distortions of the attached water molecules also display a slight response in the ZFS. The result validates earlier theoretical attempts to simulate the fluctuations of the ZFS and paramagnetic relaxation in aqueous Ni(II) solution[32].

The valence electronic shell of both Ni(II) and Mn(II) have a half-filled  $e_g$  level ( $(t_{2g})^6(e_g)^2$  and  $(t_{2g})^3(e_g)^2$  respectively), and both aqueous Ni(II) and Mn(II) possess  $T_h$  symmetry. Since there are 19 atoms, there will be 51 normal modes in total. Of these there are 15 modes of the metal-oxygen  $\text{MO}_6$  unit which are of prime importance. In this bare bone structure, where the external vibrations of the  $\text{H}_2\text{O}$  are neglected, the unit possesses  $O_h$  symmetry, and spans the irreducible representation  $\Gamma_{\text{vib}} = a_{1g} + e_g + 2t_{1u} + t_{2g} + t_{1u}$ .

A total of 51 normal modes were examined using the CASSCF method. For ease of discussion we will refer to the modes by their  $T_h$  symmetry name. Among these only a few of them are 'active' modes which display ZFS when distorted.

The  $E_g$  modes are Mn-O vibrations and the  $T_g$  modes correspond to mixed character scissoring of the oxygens, along with HOH distortions. In the case

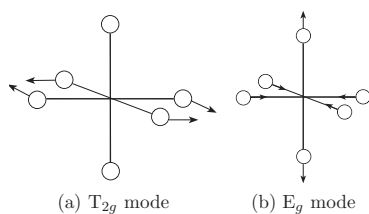


**Figure 4.3:** Showing the geometrical distortion along the a)  $T_{2g}$  (*left*) and b)  $E_g$  (*right*) normal modes of the  $MO_6$  complex in  $O_h$  symmetry.

of Mn(II) an 'active' mode was so defined if the splitting of the ground state energy levels was larger than  $0.1 \text{ cm}^{-1}$ . The frequency of the  $T_g$  is  $100 \text{ cm}^{-1}$  and of  $E_g$  is  $237 \text{ cm}^{-1}$ . There are further three  $T_g$  modes at a frequency of  $520 \text{ cm}^{-1}$  which display very slight linear response in  $D$  to distortions. Figure 4.4 and 4.5 show distortions along 5 active normal modes for the Ni(II) and Mn(II) hexa-aqua complexes respectively.

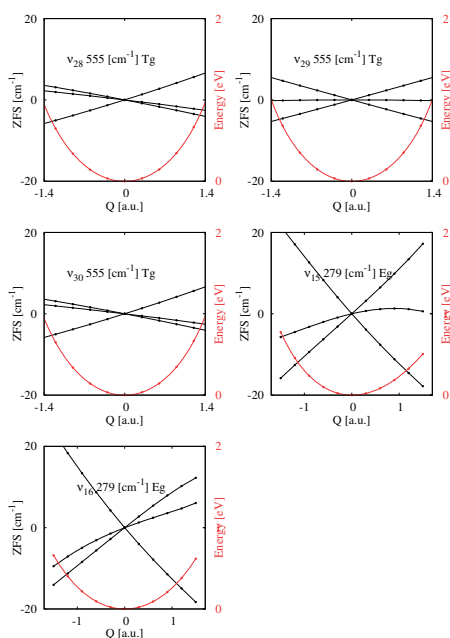


**Figure 4.4:** Showing the  $T_g$  and  $E_g$  active normal modes of Ni(II) hexa-aqua complex with distortions along the normal modes. The figure shows the splitting of the lowest ground state energies as well as the energy of the first excited state.

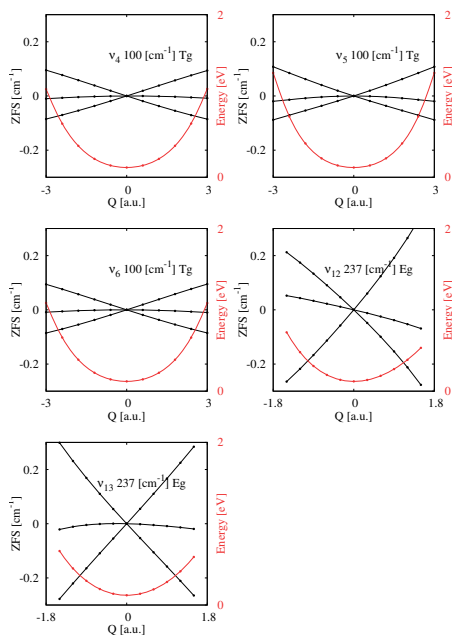


**Figure 4.5:** Showing the  $T_g$  and  $E_g$  active normal modes of Mn(II) hexaqua complex with distortions along the normal modes. The figure shows the splitting of the lowest ground state energies as well as the energy of the first excited state.

## 4.2 ZFS parameters from Density Functional Theory

We did various tests to determine the accuracy of the DFT formalism to compute the ZFS on  $\text{Gd(III)F}_6^{3-}$  and  $\text{Gd(III)H}_2\text{O}_6^{3+}$ . It was found that the DFT results are highly functional dependent and in particular the hybrid functionals are rather inaccurate when compared to CASSCF results, the error of which increases as a larger amount of Hartree-Fock exchange is added to the functional (for example, the amount of HF energy in increasing order: TPSSH < PBE0 < B3LYP). To compare directly to experimental values we ran DFT computations on the compound  $\text{Gd(III)DTPA}^{2-}$  which has an experimental  $D$  parameter of  $0.048 \text{ cm}^{-1}$  and  $E/D=0.2$ [33]. The DFT results for the Coupled-Perturbed (CP)[34] and Pederson-Khanna (PK)[35] method using various hybrid and non-hybrid functionals is shown in Table 4.1. The computed  $D$  values seem unrealistic compared to the experimental values and are highly functional dependent regardless of whether the PK or CP method is used. The DFT formalism to compute the ZFS parameters was therefore deemed unreliable especially as compared to the post-HF methods discussed in the next sections. However, it should be pointed out that DFT does have

a significant edge when considering computational speed and therefore it is important to improve DFT methods to use for dynamical sampling where a tremendous amount of calculations may be needed [36].

**Table 4.1:** Gd(III)DTPA<sup>2-</sup> ZFS parameters as computed using the DFT formalism. The experimental  $D$  value is  $0.048 \text{ cm}^{-1}$  and  $E/D = 0.2$ [33]

	CP		PK	
	$D [\text{cm}^{-1}]$	$E/D$	$D [\text{cm}^{-1}]$	$E/D$
B3LYP	1.720	0.127	1.200	0.007
BLYP	-0.193	0.123	1.299	0.007
BP86	-0.185	0.140	-0.166	0.054
PBE0	2.418	0.285	1.717	0.221

To prove this hypothesis, we ran various tests on a complex Gd(III)(HPDO3A)(H<sub>2</sub>O) for which experimental data is available, using both DFT and CASSCF and compare and contrast the two. It was found that when dealing with the static  $D_S$  one can get much better agreement with experimental results when using long-range functionals rather than, let's say for example TPSS (but of course not a hybrid functional as is noted earlier). In particular the LC-BLYP functional was investigated and the results comparing the various functionals and methods to experiment is shown in Table 4.2. We then show the correlation between CASSCF and TPSS and the comparison between CASSCF and LC-BLYP, and found that there is little to no correlation, the Pearson values being close to zero in both cases. (The Pearson value is a measure of correlation, 1 being totally correlated, -1 meaning perfect anti-correlation and 0 being no correlation at all).

**Table 4.2:** Static ZFS parameters in  $\text{cm}^{-1}$  of [Gd(III)(HPDO3A)(H<sub>2</sub>O)]

	$D_S$	$E_S/D_S$	$\Delta_S [\text{rad s}^{-1}]$
CP-TPSS*	-0.296	0.087	$4.60 \times 10^{10}$
PK-TPSS*	-0.200	0.093	$3.12 \times 10^{10}$
LC-BLYP	-0.069	0.182	$1.12 \times 10^{10}$
CASSCF	-0.048	0.16	$0.77 \times 10^{10}$
Exp.[37]			$0.99 \times 10^{10}$

\*Values obtained by Lasoroski et al.[36]

Although the LC-BLYP functional provides a better estimation of the static ZFS, there is little to no correlation between any of the DFT methods and CASSCF as can be seen in Figure 4.6 which shows the correlation of the  $D$  parameter between CASSCF and DFT sampled over an AIMD simulation (the

details of the simulation are described in Paper II).

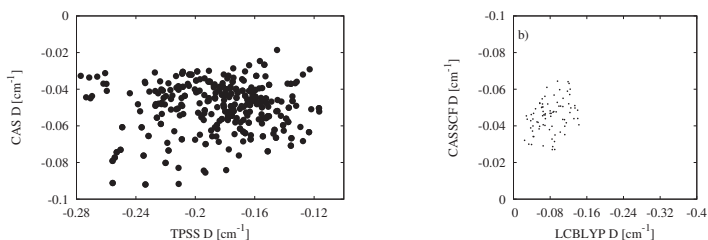


**Figure 4.6:** *left)* Correlation of  $D$  parameter between CASSCF and DFT calculations sampled over an AIMD simulation with corresponding geometries. *right)* A comparison of the total  $D$  parameter using the LC-BLYP functional compared to corresponding CASSCF geometries sampled over an AIMD simulation.

## 4.3 Paramagnetic ions in water: Aqueous Gd(III) and Eu(II)

### 4.3.1 Comparing the Zero-Field splitting for the isoelectronic aqueous Gd(III) and Eu(II)

In Figure 4.7 the splitting of the ground state octet into kramer doublets is depicted for the various complexes  $M(\text{H}_2\text{O})_n$  where  $M$  is Eu(II) or Gd(III), and the corresponding lowest lying excited sextet states are shown on the right hand side. For the case of Gd(III) the 9 co-ordinated complex has the lowest amount of splitting ( $0.0838 \text{ cm}^{-1}$ ) and from the splitting it can be seen that the  $D$  parameter is negative, whereas the  $D$  parameter is positive for the 7 or 8 co-ordinated complex. The excited state sextet of the 9 co-ordinated complex lies the highest in energy relative to the ground state at  $40285 \text{ cm}^{-1}$  compared to the 8 co-ordinated complex ( $40253 \text{ cm}^{-1}$ ) and the 7 co-ordinated complex ( $40254 \text{ cm}^{-1}$ ). The order of the lowest lying excited state corresponds directly to the splitting of the ground state: the larger the energy difference between the ground states octet and the lowest sextet excited state, the smaller the ZFS.

In the case of Eu(II) the least amount of splitting of the ground state occurs in the 8 co-ordinated complex, followed by the 9 co-ordinated complex and the 7 co-ordinated complex. Similar to the Gd(III) complexes the splitting of the ground state has a direct relation to the energy levels of the excited states. In general, the  $D$  parameters of the Eu(II) complex are much less than at least half the  $D$  parameters of the corresponding Gd(III) complexes. Whereas the

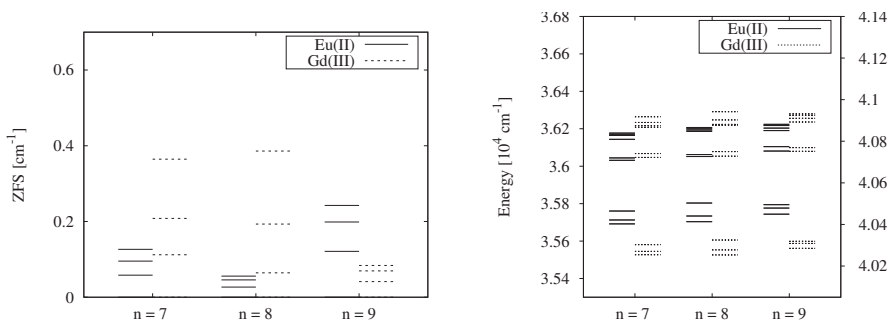


**Figure 4.7:** A comparison of optimized  $M(\text{H}_2\text{O})_n$  complex where  $M$  is  $\text{Eu}(\text{II})$  or  $\text{Gd}(\text{III})$  and  $n = 7, 8$  or  $9$ . The left-hand figure shows the splitting of the ground state octet. The right-hand figure shows the lowest excited state sextets where the left axis corresponds to  $\text{Eu}(\text{II})$  and the right axis corresponds to the energy values for  $\text{Gd}(\text{III})$ .

$\text{Gd}(\text{III})$  complexes have the lowest lying excited states close to approximately  $40200 \text{ cm}^{-1}$ , the lowest lying excited states of the  $\text{Eu}(\text{II})$  complexes are much lower in energy around the  $35700 \text{ cm}^{-1}$  mark. Surprisingly, despite the  $\text{Eu}(\text{II})$  and  $\text{Gd}(\text{III})$  ions being iso-electronic there is no systematic trend in the ZFS for each system size.

**Table 4.3:**  $D[\text{cm}^{-1}]$  and  $E/D$  values for  $M(\text{H}_2\text{O})_n^{3+}$ ,  $M = \text{Eu}(\text{II})/\text{Gd}(\text{III})$  and  $n = 7, 8, 9$

$\text{Gd}(\text{III})(\text{H}_2\text{O})_n^{3+}$	$n = 7$	$n = 8$	$n = 9$
D	0.027124	0.032175	-0.006978
E/D	0.230687	0.000	0.006169
$\text{Eu}(\text{II})(\text{H}_2\text{O})_n^{2+}$	$n = 7$	$n = 8$	$n = 9$
D	-0.009773	-0.004633	-0.019978
E/D	0.175659	0.000	0.059986
Gd@Eu	$n = 7$	$n = 8$	$n = 9$
D	0.020426	0.023069	-0.006743
E/D	0.108761	0.000	0.242639
Eu@Gd	$n = 7$	$n = 8$	$n = 9$
D	-0.038871	-0.069411	0.019791
E/D	0.162949	0.000	0.004493

To investigate the differences in  $\text{Eu}(\text{II})$  and  $\text{Gd}(\text{III})$ , we decided to use the  $\text{Eu}(\text{II})$  optimized geometry and replace the metal center with  $\text{Gd}(\text{III})$  and vice versa and see the effect this would have on the splitting of the ground state.

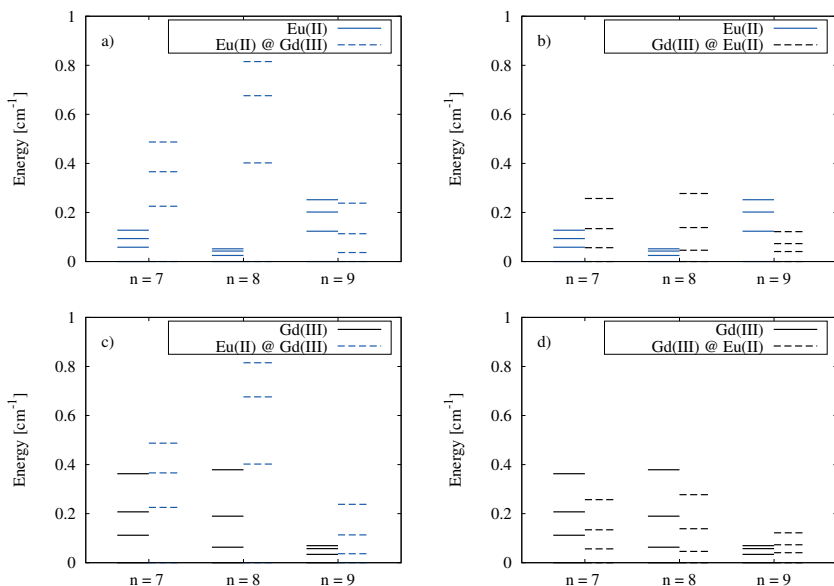


**Figure 4.8:** A comparison of the splitting of the ground state octet when interchanging the paramagnetic center at different geometries. A@B corresponds to using A as the metal ion center whilst using the optimized geometry of B.

This would give us deeper insight into the nature of the ZFS since Eu(II) and Gd(III) are iso-electronic and allow us to see the sensitivity of the splitting to the geometry under consideration. The results are depicted in Figure 4.8 where A@B corresponds to using A as the center while using the optimized geometry of the complex B. In panel a) we see that in the case of Eu(II), changing the geometry to the Gd(III) optimized geometry has a dramatic effect on the 7 and 8 co-ordinated complexes, increasing the splitting from  $0.1264 \text{ cm}^{-1}$  to  $0.4979 \text{ cm}^{-1}$  and from  $0.0557$  to  $0.8334 \text{ cm}^{-1}$  respectively, while the 9 co-ordinated complex remains almost the same, and decreasing only slightly from  $0.2425 \text{ cm}^{-1}$  to  $0.2237 \text{ cm}^{-1}$ . The least splitting for the Eu(II) metal center is witnessed with the 8 co-ordinated complex whereas, in the case of Gd(III) the lowest amount of splitting occurs in the 9 co-ordinated complex. In panel d) for the case of Gd(III), changing the geometry to Gd@Eu lowers the total amount of splitting of the ground state octet in the case of the 7 and 8 co-ordinated complex from  $0.3646 \text{ cm}^{-1}$  to  $0.2536 \text{ cm}^{-1}$  and from  $0.3861 \text{ cm}^{-1}$  to  $0.2768 \text{ cm}^{-1}$  respectively, whereas for the 9 co-ordinated complex the splitting is increased very slightly from  $0.0838 \text{ cm}^{-1}$  to  $0.0912 \text{ cm}^{-1}$ . The  $D$  values for the various complexes are shown in Table 4.3

Overall, we see that changing the geometry has a more dramatic effect on Eu(II) as compared to Gd(III). Replacing Gd(III) at the Eu(II) cluster geometries shows the same trend as Figure 4.7.

#### 4.3.2 AIMD trajectory: Comparison of inner and outer shell in aqueous Gd(III)

We performed an ab-initio MD simulation (AIMD) on a Gd(III) complex with 98 water molecules. From the trajectory of our AIMD simulation on aqueous Gd(III), we extracted several snapshots using the first shell with a cut-off radius of 3 Å which on average included 8 water molecules and the second shell with a cut-off of 5 Å which included a total of 22-24 water molecules. The values for the inner and outer shell are determined from the radial distribution function (RDF) in Figure 4.9 which presents the paramagnetic Gd(III) complex in aqueous solution from classical and AIMD simulations. The classical MD simulation used varying box sizes and included a single, double and triple Gd(III) ions in the simulation. From the AIMD simulation the peak of the first hydration shell was acquired at a distance of 2.45 Å for the case of aqueous Gd(III) and integration of the first peak gives a coordination number  $n(r)$  of 8.0 for Gd(III).

These cluster configurations from a limited sampling of the AIMD simulation were used to compare the effect of including the second shell on the ZFS. The comparison of the 2nd Kramers Doublet energies of the two configuration samples is depicted in Figure 4.10. We see that though the points deviate slightly from perfect correlation, the effect of the second-shell is quite small and considering the balance between accuracy and statistical sampling, it is much more computationally efficient to only include the first shell in the calculations.

## 4.4 Paramagnetic Complexes of Clinical Relevance

### 4.4.1 Static ZFS in Gd(III)DOTA(H<sub>2</sub>O)<sup>-</sup> and Gd(III)DTPA(H<sub>2</sub>O)<sup>2-</sup>

Two complexes that are of relevance to paramagnetic-NMR experiments: the Gd(III)DOTA(H<sub>2</sub>O)<sup>-</sup> and Gd(III)DTPA(H<sub>2</sub>O)<sup>2-</sup> complexes are presented here, which form the first generation of clinical contrast agents for use in medical MRI. Experimental ZFS parameters may vary since the acquisition is performed under dynamical conditions; molecular vibrations and solvent collisions may effect the result. It is for this reason that we have used several geometries to acquire the ZFS. We have used previously reported optimized

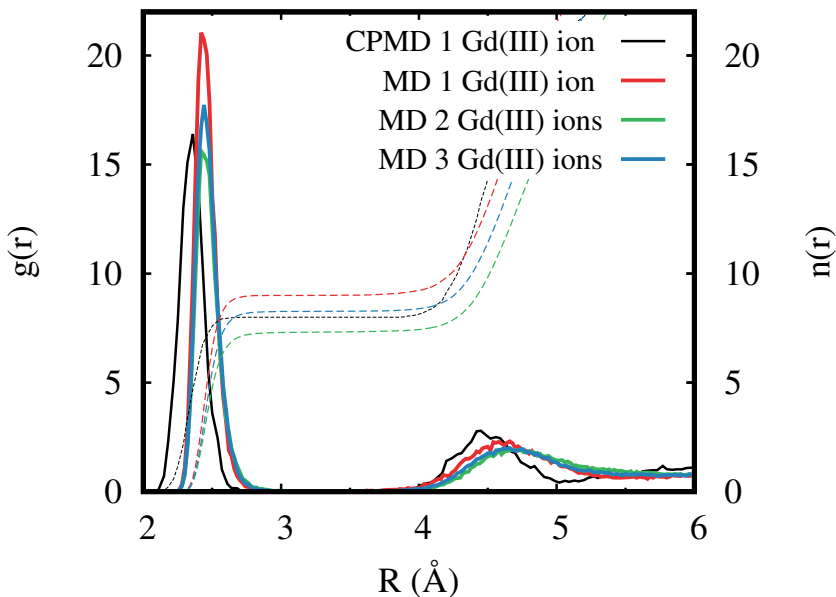


**Figure 4.9:** Radial distribution functions,  $g(r)$ , and cumulative coordination numbers,  $n(r)$ , of the paramagnetic Gd(III)- oxygen distance from the MD simulation (containing one, two and three Gd(III) ions in a periodic box) and from the AIMD simulations of aqueous Gd(III).

geometries under the TPSSh functional for the  $\text{Gd(III)DOTA(H}_2\text{O)}^-$  and  $\text{Gd(III)DTPA(H}_2\text{O)}^{2-}$  [38] along with optimizing these structures with the B3LYP functional.

**Table 4.4:** Comparing the *ab-initio* ZFS [ $\text{cm}^{-1}$ ] from CASSCF/MRCIO calculations to previously reported experimental values

	Exp. Value	TPSSh geom	B3LYP geom
$\text{Gd(III)DOTA(H}_2\text{O)}^{2-}$	0.230 [33]	0.179	0.100
$\text{Gd(III)DTPA(H}_2\text{O)}^{2-}$	0.576[33]	0.592	0.375

Figure 4.11, shows a comparison of the splitting between the Kramer doublets of the two complexes as well as the ZFS splitting obtained from the  $D$  values as shown in Figure 2.1, where rhombic contributions  $E$  are neglected. The experimental splittings, corresponding to  $12D$ , for  $\text{Gd(III)DOTA(H}_2\text{O)}^-$  and  $\text{Gd(III)DTPA(H}_2\text{O)}^{2-}$  of 0.23 and 0.576  $\text{cm}^{-1}$  respectively are in reasonable agreement with those obtained using the TPSSh optimized

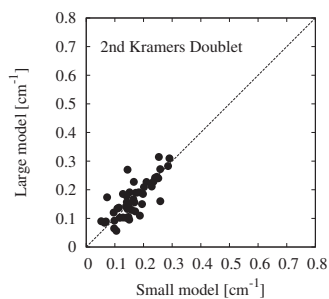


**Figure 4.10:** A comparison of the 2nd Kramer Doublets of the ground state energy between the inner shell Gd(III) and the inclusion of the outer shell in the aqua complex.

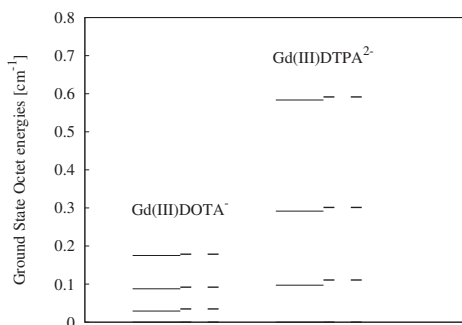


**Figure 4.11:** Ground Octet State Splitting of the Kramer Doublets: a comparison of the two systems of interest. The CASSCF/MRCI0 values are shown as solid lines whereas the *D*-derived cylindrical values are shown as dashed lines.

structure as can be seen from Table 4.4. It is clear that certain discrepancies arise due to the sensitivity to geometry and a more extensive sampling may provide deeper insight. However, the overall scheme produces reasonable estimates. In Figure 4.11, we notice that there are also limitations of the second order formulation of the spin-Hamiltonian, since the  $D$  and  $E$  values fitted to the ZFS splitting tensor are not exactly aligned with the splitting of the exact Kramer doublets.

Next, we consider the dynamic effects of  $\text{Gd(III)DOTA(H}_2\text{O)}^-$  by distorting the distance of the water molecule from the Gd(III) center and viewing the resulting fluctuations in the ZFS. Three geometry structures were used: one experimental [39], a previously reported optimized structure using the TPSSh functional [38] and one optimized using the B3LYP functional.

**Table 4.5:** ZFS parameters from CASSCF/MRCI0 calculations using various geometries for the  $\text{Gd(III)DOTA}^-$  and  $\text{Gd(III)DOTA(H}_2\text{O)}^-$

	Exp.Geom	Supp (TPSSh)	Optimized (B3LYP)	Exp. Value
$\text{Gd(III)DOTA}^-$				
$D$ value [ $\text{cm}^{-1}$ ]	0.050	0.033	0.028	
$E/D$	0.219	0.013	0.004	
Splitting [ $\text{cm}^{-1}$ ]	0.662	0.398	0.330	
$\text{Gd(III)DOTA(H}_2\text{O)}^-$				
$D$ value [ $\text{cm}^{-1}$ ]	0.028	0.015	0.078	-0.019
$E/D$	0.226	0.081	0.165	
Splitting [ $\text{cm}^{-1}$ ]	0.370	0.179	0.100	0.230

Experimental values for the ZFS  $D$  parameter of  $\text{Gd(III)DOTA(H}_2\text{O)}^-$  have been reported as  $-0.019 \text{ cm}^{-1}$  which results in a maximal multiplet splitting of  $0.23 \text{ cm}^{-1}$  assuming that the complex maintains axial symmetry[33]. We were unable to reproduce the negative sign of  $D$ . However, the negative value is of little significance to actual electronic spin relaxation calculations since the square of terms is required for the equations, but it is of principal importance for the calibration of the calculations. Currently it is difficult to assess whether there is any structural relation to the sign of the ZFS parameter.

The CASSCF/MRCI0 calculations follow the relationship of the spin

Hamiltonian formalism and maintain a splitting of  $2D$ ,  $4D$  and  $6D$ , yet our value of  $D > 0$ , is in contrast to experimental work. From Table 4.5 we see that depending on the geometry of the complex we should expect a variation of the total induced splitting. From the reference experimental value of  $0.23 \text{ cm}^{-1}$  the most representative geometries seem to be generated from the TPSSh functional as presented in reference [38] and our treatment produces a total splitting of  $0.1787 \text{ cm}^{-1}$ , which lies close to the experimental range. Utilizing the TPSSh geometry we varied the distance of the water molecule to the central complex to see the variation in the ZFS, and this is shown in Table 4.6. The variation in the  $D$  parameter is rather small and it can be concluded that the distance of the water molecule does not significantly effect the ZFS.

**Table 4.6:** ZFS parameters from CASSCF/MRCIO calculations as the Gd-O bond distance (between the connected water molecule) is increased for Gd(III)DOTA(H<sub>2</sub>O)<sup>-</sup> using the TPSSh optimized geometry

	2.646 [Å]	2.70 [Å]	2.75 [Å]	2.80 [Å]
$D [\text{cm}^{-1}]$	0.015	0.015	0.016	0.016
$E/D$	0.081	0.050	0.033	0.023
Splitting [ $\text{cm}^{-1}$ ]	0.179	0.181	0.188	0.200

#### 4.4.2 Static and Transient ZFS in Gd(III)(HPDO3A)(H<sub>2</sub>O): combining classical and quantum methods

In Gd(III) contrast agents the relaxation of the electron spin to a large extent dominates the paramagnetic relaxation enhancement of nuclear spins. The electronic spin relaxation is driven by the magnitudes of the static and transient ZFS ( $\Delta_S$  and  $\Delta_T$  respectively), the correlation time of the Brownian rotational motion of the complex ( $\tau_2$ ) and the correlation time of the transient ZFS ( $\tau_v$ ). For a more complete discussion on how these parameters modulate the electronic spin relaxation, please refer to Section 3.5. Here we discuss the clinical complex [Gd(HPDO3A)(H<sub>2</sub>O)], the structure of which is shown in Figure 4.12. From an AIMD trajectory we were able to extract a configuration space sampling that consisted of four blocks (90 X 4 snapshots) of 0.57 ps each. The configuration snapshots were the same as those sampled for DFT by Lasoroski et al.[36]. The AIMD trajectory consisted of a single Gd(III)HPDO3A(H<sub>2</sub>O) central complex in a 15.4 Å cubic box solvated by 98 water molecules.

As opposed to calculating the static ZFS from an optimized geometry as

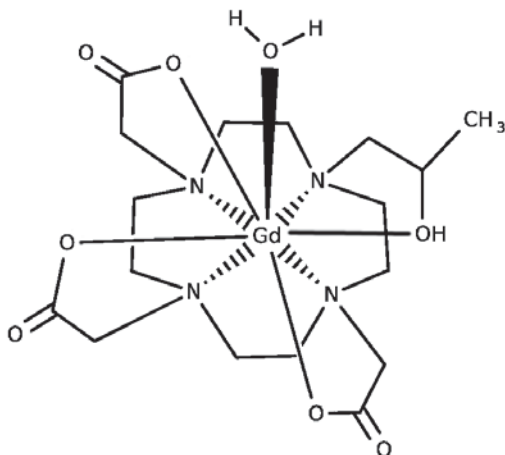


**Figure 4.12:** Schematic structure of  $[\text{Gd}(\text{HPDO3A})(\text{H}_2\text{O})]$  contrast agent showing the 9-fold coordination of the paramagnetic central Gd(III) ion

was done in Section 4.4.1, here the static ZFS is computed by averaging over the entire configuration space sampling, both for each element of the static  $\bar{D}_S$  tensor as well as the total magnitude ( $\Delta_S$ ). The values obtained for the  $D$ ,  $E/D$  parameters and the corresponding magnitude ( $\Delta_S$ ) from our calculations as well as experimental values are shown in Table 4.7.

**Table 4.7:** Static ZFS parameters in  $\text{cm}^{-1}$  of  $[\text{Gd}(\text{HPDO3A})(\text{H}_2\text{O})]$

	$D_S$	$E_S/D_S$	$\Delta_S$ [ $\text{rad s}^{-1}$ ]
CASSCF	-0.048	0.16	$0.77 \times 10^{10}$
Exp.[37]			$0.99 \times 10^{10}$

In Fig. 4.13, the correlation between the octet Kramer doublet levels and the  $D$  parameter for the CASSCF sampled over the AIMD trajectory is presented. There is a nearly linear relationship between the  $D$  parameter and the energy levels arising from the splitting of the ground state. The limited influence of the rhombic  $E$  parameter is seen in the small spread of the higher Kramer doublet levels. The splitting of the ground state octet determines the sign of the  $D$  parameter as is explained in Section 2.1. In the case of  $[\text{Gd}(\text{III})(\text{HPDO3A})(\text{H}_2\text{O})]$ , it forms a negative  $D$  parameter. The values of  $D$  vary from  $-0.10 \text{ cm}^{-1}$  to  $-0.02 \text{ cm}^{-1}$ , and the splitting of the highest ground state octet varies from  $0.40 \text{ cm}^{-1}$  to  $1.20 \text{ cm}^{-1}$ . Fig. 4.14a shows the  $D$  parameter evolve over a single block of 0.57 ps and Fig. 4.14b shows the splitting of the ground state octet energy levels.

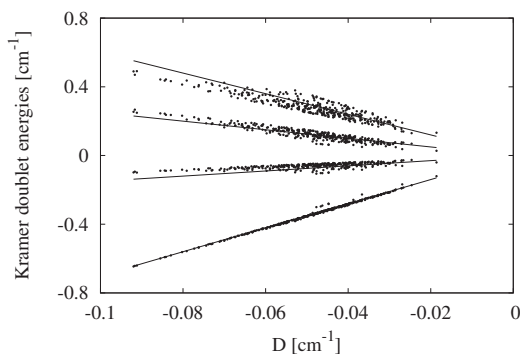


**Figure 4.13:** Relationship between the  $D$  parameter(x-axis) and the relative energies of Kramer doublet ground state energy levels(y-axis)

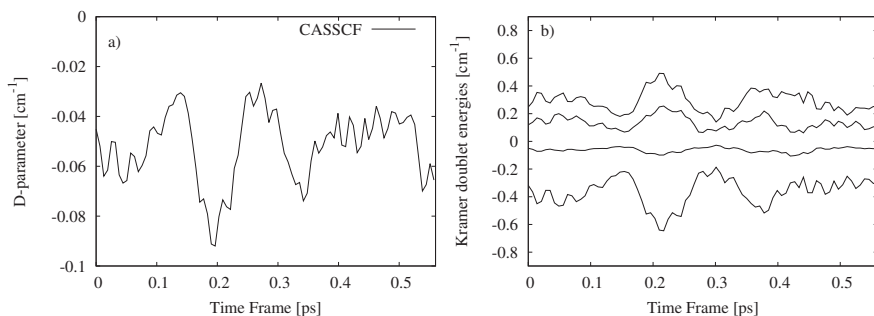


**Figure 4.14:** a) evolution of the  $D$  parameter using CASSCF b) Time evolution of the splitting of the octet ground state into Kramer doublets using CASSCF, sampled along the AIMD trajectory for a single block over 0.57 ps for the hydrated [Gd(III)(HPDO3A)(H<sub>2</sub>O)].

For CASSCF the diagonal elements  $(d_{11}, d_{22})$  and  $(d_{22}, d_{33})$  exhibit a linear correlation, with Pearson values for  $(d_{11}, d_{22})$ ,  $(d_{11}, d_{33})$  and  $(d_{22}, d_{33})$  being 0.55, -0.51, -0.70, respectively. This appears to be related to the fact that the transient matrix element  $d_{33}$  remains static, close to a value of 0, and since the ZFS tensor is traceless, there is a correlation in  $(d_{11}, d_{22})$  which compensates for the nearly static value of  $d_{33}$ . In spite of this correlation when computing the time correlation function (TCF), we assume that the elements  $d_{ij}$  are uncorrelated. From the TCF of the transient  $\bar{D}_{trans}(t)$  we can calculate a characteristic time scale of the fluctuations that influence the spin dynamics. The average of the normalized auto-correlation function has been computed

using all nine coefficients of the ZFS tensor:

$$C(t) = \frac{1}{9} \sum_{i,j} \frac{\langle d_{ij}(0)d_{ij}(t) \rangle}{\langle d_{ij}(0)d_{ij}(0) \rangle} \quad (4.1)$$

The results for  $C(t)$  derived from the CASSCF calculations are shown in Figure 4.15. The data points can be fit to an oscillatory and exponentially decaying curve of the form  $\exp(-t/\tau_c)\cos(2\pi\nu t)$  which gives a correlation time  $\tau_c$  of 63.8 fs and a characteristic frequency  $\nu$  of  $199.5 \text{ cm}^{-1}$ .

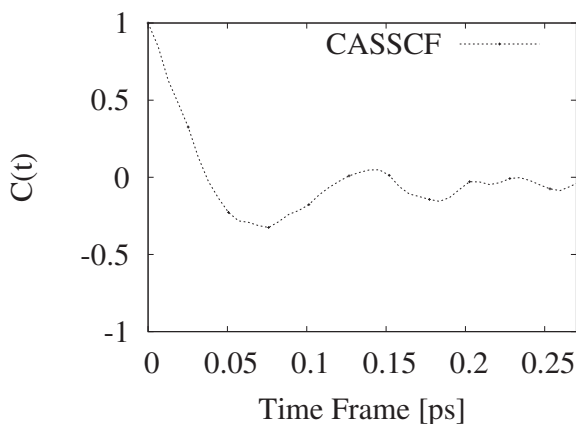


**Figure 4.15:** Time correlation function  $C(t)$  of the ZFS tensor, as defined in Eq. 4.1.

## 5. Conclusions and Outlook

In this thesis we have used Molecular Dynamics (MD) simulations along with Quantum Chemical (QC) computations in order to get a step closer to computing the electron spin relaxation parameters at the highest level of theory possible today. The *ab-initio* calculations using post-Hartree Fock methods are the first of its kind on any of the lanthanide complexes and set a new precedent for accurate computations. A careful assessment is made against experimental parameters which shows promising results for the Complete Active Space Self-Consistent Field (CASSCF) method. Furthermore, we show that the addition of dynamical correlation effects, via the n-electron valence state perturbation theory (NEVPT2) method, has a limited influence on the Zero-Field Splitting (ZFS).

We reviewed Density Functional Theory (DFT) and the CASSCF methods in order to compute the ZFS of various paramagnetic complexes, starting from simple structures to more complex ones. It is found that DFT is highly functional dependent. In particular, the results vary more erratically, the greater the amount of Hartree-Fock (HF) exchange is added to a hybrid functional, and so it is suggested that non-hybrid functionals be used and in particular long-range corrected functionals perform significantly better when comparing to experimental estimates of the static ZFS. This may be due to the fact that long-range DFT corrections influence the Kohn-Sham (KS) orbitals and therefore subsequently influence the ZFS. The CASSCF method, on the other hand, seems to be a reliable indicator of the scale of the static ZFS. This difference in methods may possibly be attributed to the way in which the  $\bar{D}$ -tensor is computed. DFT is unable to handle the multi-determinantal character of the spin eigenfunctions involved in the ZFS, and the ZFS tensor is evaluated to reconstruct the model spectrum *a posteriori*. Therefore, in DFT the excited states spin-orbit (SO) coupling to the ground state are only implicitly and approximately treated. In the HF-method the multideterminantal character of the ground state is not well described and an important portion of the electron correlation is omitted. The hybrid DFT functional compensates for this by mixing the accurate description of the exchange from HF with the useful approximations for correlation from DFT. In CASSCF the ZFS computation proceeds in two steps: (i) a set of spin-orbit free states is computed at the CASSCF level (ii) the low-lying spin-orbit spectrum

can be computed directly through a state interaction (SI) method.

Through a rigorous analysis of the comparison between CASSCF and DFT, it was found that none of the DFT functionals correlates with the CASSCF method when computing the static ZFS. This was made possible by performing ZFS computations on approximately 400 configuration snapshots produced from an *ab-initio* Molecular Dynamics (AIMD) trajectory. Since we have indications that CASSCF is rather accurate, we conclude that none of the versions of DFT is reliable, even though the magnitude may be improved for some functionals. On the other hand, when analysing the correlation time of the transient  $\bar{D}$ -tensor, one obtains values that are of a similar time-scale using CASSCF and DFT, which show a faster decay than experimental estimates.

It was shown that for aqueous Gd(III), inclusion of the inner solvation shell is sufficient in accurately producing the ZFS, and the computational cost of including an outer shell in the calculations has only a limited influence on the outcome and so is deemed too expensive at the moment. This result, that only the short-range interactions dominate the ZFS, is of general importance and can be extended to any complex. When comparing static ZFS values between the iso-electronic Gd(III) and Eu(II) (both containing 7 electrons in the *f*-orbital) no systematic trend was found between the complexes, which reveals the difficulty in determining the origin of the ZFS. We also performed studies on paramagnetic Ni(II) and Mn(II) hexa-aqua complexes, which was an extension of earlier studies. Juha Vaara et al. have shown that CASSCF can be used to study paramagnetic nuclear spin relaxation and electron spin relaxation parameters for Ni(II) in solution [40–43]. Against the backdrop of their studies, we show that a normal mode analysis can be an efficient approach to study ZFS fluctuations, since the problem can be projected in terms of a few intra complex coordinates. This gives an insight into the geometry dependence of the ZFS and a convenient ZFS property surface which can be used for MD simulations. Hence, with a ZFS property function along the normal modes, the ZFS in any nearly octahedral configuration can be predicted. Therefore, CASSCF calculations at each time instance is not required, and one could instead get fully converged time-correlation functions of the ZFS for use in spin simulations simply based on classical MD performed on the scale of micro or milliseconds. In the future the normal mode analysis could be evaluated for distorted configurations from MD simulations for explicit ZFS(t) calculations. Furthermore, one could anticipate a similar normal mode analysis on lanthanide complexes and so the current Ni(II) and Mn(II) study could serve as a useful reference point.

As computational power increases, using an extended active space (currently for Gd(III) and Eu(II) we use 7 electrons in 7 orbitals) as well as "post-CASSCF" methods such as multi-reference configuration interaction

(MRCI), may make it possible to evaluate the ZFS parameters with more confidence. Future studies on lanthanide and actinide complexes (both as molecular liquids and solid-state complexes for which Electron Paramagnetic Resonance (EPR) experimental values are available) will reveal how accurately the ZFS can be reproduced. An extended classical MD simulation over the scale of nanoseconds may make it possible to witness direct water exchange in the inner shell of aqueous lanthanide complexes, therefore filling in an important piece of spin relaxation parameters directly through theory. We evaluated three real Magnetic Resonance Imaging (MRI) contrast agents (ProHance, Dotarem and Magnevist), and in the future one could also anticipate *ab-initio* studies of MRI contrast agents of paramagnetic ions coordinated to biomolecules, which can give valuable input to experiments. Furthermore, the calculation of paramagnetic shielding parameters can be anticipated directly through first principles for the lanthanide series, since the  $\bar{D}$ -tensors and  $g$ -tensors for various Gd(III) complexes have been computed.



# Acknowledgements

I would like to acknowledge the help of my supervisors Michael Odelius and Jozef Kowalewski who have assisted me greatly with my research and every small issue that I may have faced during my PhD. Michael Odelius has been an inspiration not only because of his scientific achievements, but also as a kind and generous human being. I would like to thank Vladimir Malkin and Olga Malkina for allowing me to work in their laboratory in the summer of 2014. Giacomo Parigi and Claudio Luchinat were kind enough to let me work at their lab in Florence, and I am grateful to them for their guidance. I would also like to thank the members of our group Ida, Emelie, Jesper and Naresh for their discussions as well as the support of the Chemical Physics laboratory. I would like to thank Rodolphe Pollet for the collaboration with his laboratory. Ria Broer and Remco Havenith kindled my interest in the subject of quantum chemistry during my masters degree and I am ever grateful to them both. I would like to thank my doctors Eva and Maria, and my caretaker Georg Dester for their support, and I would like to thank the members of the HR team at the Physics Department for their assistance. Finally, I am forever indebted to my brother, father, Manal and Erica without who I would probably not be able to survive the conditions of the thesis writing. I acknowledge financial support from the Marie-Curie ITN. The research leading to these results has received funding from the People Programme (Marie Curie Actions) of the European Union's Seventh Framework Programme FP7/2007-2013/ under REA Grant Agreement No. 317127.



# Populärvetenskaplig sammanfattning

Magnetisk resonanstomografi (MR) kan avbilda olika organ och ben inne i kroppen och används allmänt inom medicin. Detta beror på att det är en icke-invasiv teknik (till skillnad från andra metoder för bilddiagnostik som tex. röntgen). Innan en MR-skanning utförs tas ofta ett Gadolinium-baserat kontrastmedel av patienten. Detta kontrastmedel förbättrar upplösningen i avbildningen av mjuk vävnad. Syftet med denna avhandling är att sträva efter att förstå vad som orsakar den förbättrade upplösningen genom att undersöka en viss process som kallas "elektronspinrelaxation".

Två huvudgrenar av modern fysik har använts: kvantmekanik och klassisk mekanik. Även om kvantmekanik är en mer exakt metod så är det, på grund av beräkningskostnader, inte alltid möjligt att utföra dessa beräkningar på stora system som rör sig i tiden. De flesta moderna tillvägagångssätt inom teknik bygger på klassisk fysik. Till exempel, för att beräkna spänningen eller belastningen av balkar i en fast struktur inom arkitektonisk teknik behöver man inte oroa sig för kvantmekaniska effekter, utan kan uteslutande använda sig utav klassisk mekanik. Direkt kvantmekaniska effekter börjar bli betydelsefulla när vi går ner på molekylär eller atomär längdskala. Om vi tittar på ett molekylärt system som förändras i tiden, kan atomernas rörelser approximeras som olika vibrationer, rotationer och kollisioner med varandra. För att spara beräkningskostnader kan detta beskrivas med klassisk mekanik. Vi kan följa banorna för dessa virvlande atomer över tiden och kan ta momentana bilder av atomernas positioner, som vi betraktar som ögonblicksbilder av rörelsen. Varje ögonblicksbild kan användas för att kvantmekaniskt beräkna olika statistiska egenskaper av intresse. Förutom kvantmekanik används även Einsteins speciella relativitetsteori. Detta på grund av att systemen vi är intresserade av är uppbyggda av tunga atomer och elektronerna i vissa lägen rör sig nära ljusets hastighet. Under dessa förutsättningar blir relativistiska effekter viktiga. Kombinationen av klassisk mekanik och kvantmekanik utgör den grundläggande metodiken som har använts i denna avhandling.

”Så vad är poängen?”, kanske du frågar. Jo, denna slags forskning är viktig av två skäl: för det första kan den bidra till framställning av nya förbättrade

kontrastmedel. För det andra, och kanske även viktigare, testar den gränserna för vad som är möjligt att beräkna dessa dagar.

# References

- [1] A. RAHMAN. **Correlations in the Motion of Atoms in Liquid Argon.** *Physical Review*, **136**:A405–A411, Oct 1964. 9
- [2] PIERRE HOHENBERG AND WALTER KOHN. **Inhomogeneous electron gas.** *Physical Review*, **136**(3B):B864, 1964. 10
- [3] MAX BORN AND ROBERT OPPENHEIMER. **Zur quantentheorie der molekeln.** *Annalen der Physik*, **389**(20):457–484, 1927. 16
- [4] DOUGLAS R HARTREE. **The wave mechanics of an atom with a non-Coulomb central field. Part I. Theory and methods.** In *Mathematical Proceedings of the Cambridge Philosophical Society*, **24**, pages 89–110. Cambridge Univ Press, 1928. 17
- [5] VLADIMIR FOCK. **Näherungsmethode zur Lösung des quantenmechanischen Mehrkörperproblems.** *Zeitschrift für Physik*, **61**(1-2):126–148, 1930. 17
- [6] JOHN C SLATER. **Note on Hartree’s method.** *Physical Review*, **35**(2):210, 1930. 17
- [7] ISAIAH SHAVITT. **The method of configuration interaction.** In *Methods of electronic structure theory*, pages 189–275. Springer, 1977. 19
- [8] BJÖRN O ROOS, PETER E TAYLOR, AND PER E.M. SIEGBAHN. **A complete active space SCF method (CASSCF) using a density matrix formulated super-CI approach.** *Chemical Physics*, **48**(2):157–173, 1980. 20
- [9] PIERRE HOHENBERG AND WALTER KOHN. **Inhomogeneous electron gas.** *Physical review*, **136**(3B):B864, 1964. 21
- [10] LLEWELLYN H THOMAS. **The calculation of atomic fields.** In *Mathematical Proceedings of the Cambridge Philosophical Society*, **23**, pages 542–548. Cambridge Univ Press, 1927. 21, 22
- [11] ENRICO FERMI. **Eine statistische Methode zur Bestimmung einiger Eigenschaften des Atoms und ihre Anwendung auf die Theorie des periodischen Systems der Elemente.** *Zeitschrift für Physik*, **48**(1-2):73–79, 1928. 21, 22
- [12] PAUL AM DIRAC. **Note on exchange phenomena in the Thomas atom.** In *Mathematical Proceedings of the Cambridge Philosophical Society*, **26**, pages 376–385. Cambridge University Press, 1930. 22
- [13] RICHARD P FEYNMAN. **The theory of positrons.** *Physical Review*, **76**(6):749, 1949. 22
- [14] WALTER KOHN AND LU JEU SHAM. **Self-consistent equations including exchange and correlation effects.** *Physical Review*, **140**(4A):A1133, 1965. 22
- [15] DIMITRIOS A PANTAZIS AND FRANK NEESE. **All-electron scalar relativistic basis sets for the lanthanides.** *Journal of Chemical Theory and Computation*, **5**(9):2229–2238, 2009. 23

- [16] E VAN LENTHE, JG SNIJDERS, AND EJ BAERENDS. **The zero-order regular approximation for relativistic effects: The effect of spin-orbit coupling in closed shell molecules.** *The Journal of Chemical Physics*, **105**(15):6505–6516, 1996. 23, 24
- [17] MARVIN DOUGLAS AND NORMAN M KROLL. **Quantum electrodynamical corrections to the fine structure of helium.** *Annals of Physics*, **82**(1):89–155, 1974. 23, 25
- [18] BERND A HESS. **Relativistic electronic-structure calculations employing a two-component no-pair formalism with external-field projection operators.** *Physical Review A*, **33**(6):3742, 1986. 23, 26
- [19] PAUL AM DIRAC. **The quantum theory of the electron.** In *Proceedings of the Royal Society of London A: Mathematical, Physical and Engineering Sciences*, **117**, pages 610–624. The Royal Society, 1928. 24
- [20] CH CHANG, M PELISSIER, AND PH DURAND. **Regular two-component Pauli-like effective Hamiltonians in Dirac theory.** *Physica Scripta*, **34**(5):394, 1986. 24
- [21] J-L HEULLY, INGVAR LINDGREN, EVA LINDROTH, STIG LUNDQVIST, AND A-M MARTENSSON-PENDRILL. **Diagonalisation of the Dirac Hamiltonian as a basis for a relativistic many-body procedure.** *Journal of Physics B: Atomic and Molecular Physics*, **19**(18):2799, 1986. 24
- [22] FELIX BLOCH. **Nuclear induction.** *Physical review*, **70**(7-8):460, 1946. 29
- [23] EDWARD M PURCELL, H CO TORREY, AND ROBERT V POUND. **Resonance absorption by nuclear magnetic moments in a solid.** *Physical review*, **69**(1-2):37, 1946. 29
- [24] RAYMOND DAMADIAN. **Tumor detection by nuclear magnetic resonance.** *Science*, **171**(3976):1151–1153, 1971. 29
- [25] ANIL KUMAR, DIETER WELTI, AND RICHARD R ERNST. **NMR Fourier zeugmatography.** *Journal of Magnetic Resonance (1969)*, **18**(1):69–83, 1975. 29
- [26] Z LUZ AND S MEIBOOM. **Proton relaxation in dilute solutions of cobalt (II) and nickel (II) ions in methanol and the rate of methanol exchange of the solvation sphere.** *The Journal of Chemical Physics*, **40**(9):2686–2692, 1964. 34
- [27] STÉPHANE BALAYSSAC, IVANO BERTINI, CLAUDIO LUCHINAT, GIACOMO PARIGI, AND MARIO PICCIOLI. **<sup>13</sup>C direct detected NMR increases the detectability of residual dipolar couplings.** *Journal of the American Chemical Society*, **128**(47):15042–15043, 2006. 34
- [28] IVANO BERTINI, JASMIN FARAONE-MENNELLA, HARRY B GRAY, CLAUDIO LUCHINAT, GIACOMO PARIGI, AND JAY R WINKLER. **NMR-validated structural model for oxidized *Rhodospseudomonas palustris* cytochrome c 556.** *JBIC Journal of Biological Inorganic Chemistry*, **9**(2):224–230, 2004. 34
- [29] ELIE BELORIZKY AND PASCAL H FRIES. **Simple analytical approximation of the longitudinal electronic relaxation rate of Gd (III) complexes in solutions.** *Physical Chemistry Chemical Physics*, **6**(9):2341–2351, 2004. 36
- [30] M RUBINSTEIN, A BARAM, AND Z LUZ. **Electronic and nuclear relaxation in solutions of transition metal ions with spin  $S=3/2$  and  $5/2$ .** *Molecular Physics*, **20**(1):67–80, 1971. 36
- [31] PER-OLOF WESTLUND, NIKOLAS BENETIS, AND HÅKAN WENNERSTRÖM. **Paramagnetic proton nuclear magnetic relaxation in the Ni<sup>2+</sup> hexa-aquo complex: A theoretical study.** *Molecular Physics*, **61**(1):177–194, 1987. 36
- [32] MICHAEL ODELIUS, CARL RIBBING, AND JOZEF KOWALEWSKI. **Molecular dynamics simulation of the zero-field splitting fluctuations in aqueous Ni (II).** *The Journal of Chemical Physics*, **103**(5):1800–1811, 1995. 40

- [33] MERIEM BENMELOUKA, JOHAN VAN TOL, ALAIN BOREL, MARC PORT, LOTHAR HELM, LOUIS CLAUDE BRUNEL, AND ANDRÉ E MERBACH. **A High-frequency EPR study of frozen solutions of GdIII complexes: straightforward determination of the zero-field splitting parameters and simulation of the NMRD profiles.** *Journal of the American Chemical Society*, **128**(24):7807–7816, 2006. 42, 43, 48, 50
- [34] FRANK NEESE. **Calculation of the zero-field splitting tensor on the basis of hybrid density functional and Hartree-Fock theory.** *The Journal of Chemical Physics*, **127**(16):164112, 2007. 42
- [35] MR PEDERSON AND SN KHANNA. **Magnetic anisotropy barrier for spin tunneling in Mn 12 O 12 molecules.** *Physical Review B*, **60**(13):9566, 1999. 42
- [36] AURÉLIE LASOROSKI, RODOLPHE VUILLEUMIER, AND RODOLPHE POLLET. **Vibrational dynamics of zero-field-splitting hamiltonian in gadolinium-based MRI contrast agents from ab initio molecular dynamics.** *The Journal of Chemical Physics*, **141**(1):014201, 2014. 43, 51
- [37] DANIELA DELLI CASTELLI, MARIA C CALIGARA, MAURO BOTTA, ENZO TERRENO, AND SILVIO AIME. **Combined high resolution NMR and 1H and 17O relaxometric study sheds light on the solution structure and dynamics of the lanthanide (III) complexes of HPDO3A.** *Inorganic chemistry*, **52**(12):7130–7138, 2013. 43, 52
- [38] DAVID ESTEBAN-GÓMEZ, ANDRES DE BLAS, TERESA RODRÍGUEZ-BLAS, LOTHAR HELM, AND CARLOS PLATAS-IGLESIAS. **Hyperfine Coupling Constants on Inner-Sphere Water Molecules of GdIII-Based MRI Contrast Agents.** *ChemPhysChem*, **13**(16):3640–3650, 2012. 48, 50, 51
- [39] SILVIO AIME, ALESSANDRO BARGE, FRANCO BENETOLLO, GABRIELLA BOMBIERI, MAURO BOTTA, AND FULVIO UGGERI. **A Novel Compound in the Lanthanide (III) DOTA Series. X-ray Crystal and Molecular Structure of the Complex Na [La (DOTA) La (HDOTA)]10H2O.** *Inorganic Chemistry*, **36**(19):4287–4289, 1997. 50
- [40] JIŘÍ MAREŠ, HELMI LIIMATAINEN, KARI LAASONEN, AND JUHA VAARA. **Solvation Structure and Dynamics of Ni2+ (aq) from First Principles.** *Journal of Chemical Theory and Computation*, **7**(9):2937–2946, 2011. 56
- [41] JIŘÍ MAREŠ, HELMI LIIMATAINEN, TEEMU O PENNANEN, AND JUHA VAARA. **Magnetic Properties of Ni2+ (aq) from First Principles.** *Journal of Chemical Theory and Computation*, **7**(10):3248–3260, 2011.
- [42] JYRKI RANTAHARJU, JIŘÍ MAREŠ, AND JUHA VAARA. **Spin dynamics simulation of electron spin relaxation in Ni2+(aq).** *The Journal of Chemical Physics*, **141**(1):014109, 2014.
- [43] JYRKI RANTAHARJU AND JUHA VAARA. **Liquid-state paramagnetic relaxation from first principles.** *Physical Review A*, **94**(4):043413, 2016. 56

